

EFFECTS OF BED-FORM ROUGHNESS ON LONG-WAVE
TRANSFORMATION OVER FRINGING REEFS

A THESIS SUBMITTED TO THE GRADUATE DIVISION OF THE UNIVERSITY OF
HAWAII AT MĀNOA IN PARTIAL FULFILLMENT OF THE REQUIREMENTS
FOR THE DEGREE OF

MASTER OF SCIENCE

IN

OCEAN AND RESOURCES ENGINEERING

AUGUST 2012

By

Pablo Duarte Quiroga

Thesis Committee:

Kwok Fai Cheung, Chair
Geno Pawlak
Ian Robertson

We certify that we have read this thesis and that, in our opinion, it is satisfactory in scope and quality as a thesis for the degree of Master of Sciences in Ocean and Resources Engineering.

THESIS COMMITTEE

Chairperson

ACKNOWLEDGEMENTS

I would like to thank my advisor, Prof. Kwok Fai Cheung, for his guidance, encouragement during my studies. He granted me his trust to do this work. I would like to thank my committee members Profs. Geno Pawlak and Ian Robertson for the many useful discussions, input, and support during this work.

I would like to thank Prof. Dan Cox, Dr. Tim Maddox, Jasson Killian, and the entire staff of the O.H. Hinsdale Wave Research Laboratory at Oregon State University for their support and hospitality during the laboratory experiments. I would also like to thank the Hawaii crew as well as Kim Quesnel and Jessie Willstrop, who helped with the experiments through the Research Undergraduate Experience program.

Special thanks are given to all my project team colleagues, Dr. Roeber Volker, Dr. Yoshiki Yamazaki, Megan Craw, Abdulla Mohamed, Dr. Krystian Paczkowski, Dr. Yefei Bai, and Jacob Tyler, for constructive discussions and assistance with model runs and laboratory work.

I would also like to thank those who joined me during my studies in the Department of Ocean and Resources Engineering: Dr. Krishnakumar Rajagopalan, Randi Arinaga, Jacob Foster, Justin Stopa, Kay Gemba, Troy Heitmann, Patrick James Anderson, Prof. Miguel Canals, Alejandro Sanchez, and Sophie Munger,

A mis otras dos mujeres de mi vida mi madre Rebeca y mi hermana Maira su amor siempre está conmigo

Finalmente dedico este trabajo a Jackie, esta tesis le pertenece. Su amor y amistad han hecho los últimos 10 años los mejores años de mi vida.

Financial support for my study was provided in the form of research assistantships from the National Tsunami Hazard Mitigation Program, Hawaii State Civil Defense, and the US Army Corps of Engineers. The laboratory work was supported by the National Science Foundation Grant No. 0530759 through the Network for Earthquake Engineering Simulation (NEES) program.

ABSTRACT

This thesis presents the formulation and implementation of a series of flume experiments to investigate long-wave transformation over bed-form roughness in fringing reef environments. The experiments were carried out in the Large Wave Flume at the O.H. Hinsdale Wave Research Laboratory, Oregon State University that measures 104 m long, 3.66 m wide, and 4.6 m high. A reef model has a 1:12 face slope and a long flat for investigation of wave shoaling and breaking as well as bore development and propagation. The model is 2.36 m tall and the water depth ranges from 2.36 to 2.66 m to reproduce dry and wet reef conditions. The bed-form roughness is modeled by timber beams placed across the flume in four configurations by varying the height and periodicity. The incident solitary wave height varies from 0.05 to 0.5 of the water depth to cover a range of wave breaking conditions. A series of wire and sonic gauges recorded the wave transformation along the flume for different bed roughness conditions a digital camera recorded images of the breaking waves on a background grid painted on a tank wall. The results show significant effects of the bed-form roughness on the shoaling process, the breaking water depth, and the breaking wave height on the reef slope as well as the wave height attenuation and bore speed on the reef flat.

TABLES OF CONTENTS

ACKNOWLEDGEMENTS	iii
ABSTRACT	v
LIST OF TABLES	vii
LIST OF FIGURES	viii
1. INTRODUCTION	1
2. LABORATORY MODEL.....	5
2.1 Reef configuration and roughness	5
2.2 Instrumentation and Measurements	7
3. NUMERICAL MODEL	10
4. RESULTS AND DISCUSSION.....	13
4.1. <i>Wave Shoaling</i>	13
4.2. <i>Wave Breaking</i>	15
4.3. <i>Bore Propagation</i>	17
5. CONCLUSIONS AND RECOMENDATIONS	20
REFERENCES	22

LIST OF TABLES

<u>Table</u>		<u>Page</u>
1	Sensor types and locations	25
2	Bed-form configurations	25
3	Test Conditions.	25

LIST OF FIGURES

<u>Figure</u>		<u>Page</u>
1	Fringing reef profile at Kailua, Hawaii.	26
2	Schematic of free surface flow over roughness elements on fringing reefs.	26
3	Schematic of wave flume experiments, instrumentation layout, and physical variables.	27
4	Design and installation of bed-form roughness. a) Roughness elements constructed of timber beams. b) Mounting of timber beams on 6×10 struts for installation. c) plain view of installed bedform roughness.	27
5	Photo of the installed bed-form roughness and a wired wave gauge. (b) Close-up view of the sonic and wire wave gauge.	28
6	Video capture of a breaking wave and its measurements.	28
7	Photo of a solitary wave and the correspondent raw record at wave gauge 1 (x = 17.6m).	29
8	Comparison of recorded surface elevations at wave gauge 1 (x = 17.6 m) from different trials. (a) Trial 7, 8, 23, and 24 for $H_o/h_o = 0.1$ and (b) Trials 16, 17, 32, and 33 for $H_o/h_o = 0.5$.	29
9	Time series of free surface elevation along the flume at $H_o/h_o = 0.1$ and $h_f = 0.2$ m.	30
10	Time series of free surface elevation along the flume at $H_o/h_o = 0.5$ and $h_f = 0.2$ m.	31
11	Evolution of computed and recorded free surface profiles at $H_o/h_o = 0.1$.	32
12	Evolution of computed and recorded free surface profiles at $H_o/h_o = 0.5$.	33

<u>Figure</u>	<u>Page</u>
13 Normalized crest elevation along the reef slope (X BF0, ■ BF1, ◆ BF2, ▲ BF3, ● BF4) and computed solution (- solid line) at 0 cm of water level from the flat reef.	34
14 Normalized crest elevation along the reef slope (X BF0, ■ BF1, ◆ BF2, ▲ BF3, ● BF4) and compute solution (- solid line) at 10 cm water level from the flat reef.	35
15 Normalized crest elevation along the reef slope (X BF0, ■ BF1, ◆ BF2, ▲ BF3, ● BF4) and computed solution (- solid line) at a 20 cm water level from the flat reef.	36
16 Normalized crest elevation along the reef slope (X BF0, ■ BF1, ◆ BF2, ▲ BF3, ● BF4) and computed solution (- solid line) at a 30 cm water level from the flat reef.	37
17 Wave height gradient between wg3 (x = 35.9 m) and wg7 (x = 48.2 m) on the reef slope (-X- BF0, ■ BF1, ◆ BF2, ▲ BF3, ● BF4).	38
18 Average celerity between wg3 (x = 35.9 m) to wg7 (x = 48.2 m) on the reef slope (-X- BF0, ■ BF1, ◆ BF2, ▲ BF3, ● BF4).	39
19 Wave height gradient across the wave breaker between wg7 (x = 48.2 m) and wg9 (x = 54.4 m) on the reef slope (-X- BF0, ■ BF1, ◆ BF2, ▲ BF3, ● BF4).	40
20 Wave breaking depth on the reef slope (-X- BF0, ■ BF1, ◆ BF2, ▲ BF3, ● BF4)	41
21 Breaking wave height on the reef slope. (-X- BF0, ■ BF1, ◆ BF2, ▲ BF3, ● BF4).	42
22 Wave breaking Index (-X- BF0, ■ BF1, ◆ BF2, ▲ BF3, ● BF4).	43

<u>Figure</u>	<u>Page</u>	
23	Normalized crest elevation along the flat reef (X BF0, ■ BF1, ◆ BF2, ▲ BF3, ● BF4) and computed solution (- solid line) at a 10 cm water level from the flat reef.	44
24	Normalized crest elevation along the flat reef (X BF0, ■ BF1, ◆ BF2, ▲ BF3, ● BF4) and computed solution (- solid line) at a 20 cm water level from the flat reef.	45
25	Normalized crest elevation along the flat reef (X BF0, ■ BF1, ◆ BF2, ▲ BF3, ● BF4) and computed solution (- solid line) at a 30 cm water level from the flat reef.	46
26	Wave height gradient between WG9 (x = 54.4 m) and wg14 (x =79.9 m) on the flat reef (-X- BF0, ■ BF1, ◆ BF2, ▲ BF3, ● BF4).	47
27	Average celerity between WG9 (x = 54.4 m) and WG14 (x = 79.9 m on the flat reef (-X- BF0, ■ BF1, ◆ BF2, ▲ BF3, ● BF4).	48

1. INTRODUCTION

Many tropical and sub-tropical islands in the Pacific are susceptible to flood hazards due to tsunamis, hurricanes, and high-surf events. Accurate prediction of near-shore wave conditions is of vital importance to coastal structure design, land-use planning, hazard assessment, and reef ecology. The presence of fringing reefs along these coastlines results in far more complex near-shore processes than for those with gentle slopes and sandy beaches in non-tropical environments (Gerritsen, 1981). Figure 1 shows a cross section of the reef at Kailua Bay, Oahu. The profile, which includes a steep fore reef and a reef flat delineated by the reef edge, is typical in tropical island environments. The abrupt slope transition at the reef edge introduces energetic breaking waves and subsequent bore formation and propagation over the shallow reef flat. The energy dissipation processes are complicated and augmented by the irregular reef surface with an abundance of coral heads and colonies of reef organisms (Lowe *et al.*, 2005; Nelson, 1996; and Hardy and Young 1996).

Wave breaking and dissipation in fringing reef environments has recently received attention in laboratory model studies. Nwogu and Demirbilek (2010) reported a flume experiment on transformation of random waves over a fringing reef. Roeber (2010) described two series of large-scale flume experiments at Oregon State University that included 198 tests with 10 two-dimensional reef configurations and ranges of solitary wave height and water depth. The reef configurations were modeled after the cross-shore profiles in Hawaii, Guam, and American Samoa to validate wave models for practical applications. Swigler (2009) conducted a series of basin experiments also at Oregon State University for solitary wave transformation over three-dimensional reef configurations. These experiments provided test cases for validation and calibration of the numerical

wave models and understanding of wave processes over reef geometries. However, these experiments were performed on Plexiglas or finished concrete surface without the bed-form roughness commonly found in reef environments. Lowe *et al* (2005) concluded from a field experiment at Kaneohe Bay, Hawaii that bottom friction instead of wave breaking may dominate the energy dissipation on the reef flat.

The dissipation mechanism due to free surface flows over rough beds has been a subject of research in its own right. Sleath (1987), Chen *et al* (2007), Dixen *et al* (2008), and Lowe *et al* (2008) conducted flume experiments to investigate dissipation over gravel, stone, and coral beds. Parameterized roughness geometries consisted of regularly placed pipes and triangles provide a systematic approach to examine energy dissipation in unidirectional and oscillatory flows (Mirfenderesk and Young, 2003; Ojha and Mazumder, 2010; Suntoyo *et al* 2008). Their results advance the understanding of laminar and turbulent boundary layer structures over rough beds and provide a good resource for validation of computational fluid dynamic, wave propagation, and circulation models (e.g., Fuhrman *et al* 2009; Suntoyo and Tanaka 2009; Lowe *et al* 2010). However, these flume experiments use a small roughness height compared to the water depth allowing formation of laminar and turbulent layers. The bed roughness effects are confined to a thin boundary layer allowing parameterization of the processes through a wave friction factor. The reef flat is quite shallow, usually no deeper than a few meters. The bed-form roughness might modify the flow over the entire water column and thus the wave processes in addition to energy dissipation.

Coral reef organisms form some of the most jagged surfaces in coastal waters. The frictional dissipation rates can be substantially larger than those of sandy or even rocky reef bottoms for modeling of surf-zone processes (Filipot and Cheung 2012). The height of roughness elements on the reef flat is usually of the same order of magnitude as the

water depth. The equivalent friction coefficient of bed-form roughness depends on the height, spacing, and distribution of the individual elements (Raudkivi, 1998). Researchers have used a variety of prefabricated elements or natural materials to reproduce the bed-form roughness in nearshore waters (Mirfenderesk and Young, 2003; Ojha and Mazumder, 2010; Suntoyo *et al* 2008). Figure 2 shows a schematic of bed-form roughness and its effect on the flow. For reef environments with sparse coral communities, the mean flow detaches behind a roughness element and reattaches in front of the next one. A recirculation region is formed next to the roughness element and an internal boundary layer develops. This process plays an important role on the generation of macro turbulence structures, which affect the dissipation rate as well as the flow structure of the surface waves. For shallow flows over a reef flat, the coupling between free surface and bed-form induced flows is sporadic and poorly understood.

Prior experiments on wave breaking and bore propagation have been performed over smooth or finished surface, while dissipation due to bed-form roughness has been investigated with uniform depth much greater than the roughness height. Due to coupling between bottom friction and wave breaking in shallow-reef environments, it is necessary to combine the two dissipation mechanisms in a single laboratory experiment to fully characterize the physical processes. Since scaling is an issue for these processes, physical experiments in a large flume are preferred. This study extends the fringing reef experiment of Roeber (2010) by including bedform roughness and focuses on regular bed-form roughness that can be systematically varied and parameterized under a range of flow conditions. The experiment provides measurements of solitary wave transformation from shoaling, breaking to bore propagation over roughness elements constructed of timber beams of different heights and spacing along the flume. The data allows

examination of the roughness effects on wave transformation processes and the use of a friction factor to account for bed-form roughness in fringing reef environments.

2. LABORATORY MODEL

A series of flume experiments were carried out at the O.H. Hinsdale Wave Research Laboratory at Oregon State University in summer 2009. The test facility is a National Science Foundation designated site for tsunami research within the Network for Earthquake Engineering Simulation. The controlled laboratory environment allows for a systematic investigation of the energy dissipation processes due to wave breaking and bed-form roughness as well as the modification of wave propagation characteristics.

2.1 Reef configuration and roughness

The experiments were carried out in the Large Wave Flume (LWF) that measures 104 m long, 3.66 m wide, and 4.6 m high to examine energy dissipation due to wave breaking and bed-form roughness on a two-dimensional reef model. Figure 3 shows a schematic of the flume experiments and the physical variables being measured. The prefabricated slabs of 0.2 m thickness, 3.66 m width, and 4.57 m length were mounted at bolt holes in the flume walls resulting in a 1:12 fore-reef slope and a flat reef 2.36 m above the bottom. A wedge in front of the fore reef provides a smooth transition between the 0.2-m slab and the floor of the flume. The water depth of the flume and on the reef slope and flat are denoted by h_0 , h , and h_f .

A piston-type wavemaker with a programmable hydraulic actuator is capable of generating regular or irregular waves. Researchers have used solitary waves to study shallow-water wave processes in laboratory experiments (e.g. Synolakis, 1987; Grilli *et al.* 1994, 1997; Li and Raichlen 2001; Liu *et al.* 2007; Hsiao *et al.* 2008; Roeber *et al.* 2010; Swigler and Lynett 2012). The use of solitary waves in this experiment allows precise measurements of wave transformation and energy dissipation across the reef without interference from return flows or wave setup. Waves on natural reefs with

shallow water would resemble a train of solitary waves. Synchronized measurements of the free surface elevation were made at an array of wave gauges with respect to the still water level. The incident solitary wave height is denoted by H_0 and the surface elevation from the still water level by η .

Coral reef roughness is highly inhomogeneous with varying length scales and a broad spectral distribution (Nunes and Pawlak, 2008). The structure is three dimensional and its configuration varies from location to location. For generalization and ease of installation, a geometrical representation of the bed-form roughness was made using assemblies of 2×4 timber beams across the flume at regular intervals over the reef model. This allows examination of the roughness effects in terms of generic parameters such as height and periodicity that are commonly used in hydraulic studies. Figure 4 shows a schematic of the bed-form configurations and installation. The timber beams were mounted on two 6×10 timber struts installed along the two walls. In some tests, the beams were bolted into the concrete slab for additional stability. Figure 5 shows the installed bed forms in the laboratory flume. The experiments utilized a total of 114 timber beams.

The roughness wavelength (λ) and height (k) define the pitch ratio (λ/k), which indicates the periodicity of the bed form. This type of bed-form roughness has been typically divided into d -type and k -type based on the assumption that the energy loss in the water column is due largely to the formation of wakes behind each roughness element. The vorticity in the wake may influence the turbulence characteristics in the water column depending on the pitch ratio. The d -type roughness corresponds to $\lambda/k < 2$, when the turbulence in the groove is confined and a boundary layer develops above the bed form. The flow on top of the bed-form roughness behaves similar to that over a smooth bed. This study focuses on the k -type roughness with $\lambda/k > 4$ where the higher pitch ratio results in significant shedding of turbulence into the outer flow and the effect of

individual roughness elements can be observed in the water column. Table 1 summarizes five series of laboratory experiments. These include tests with four bed-forms configurations and a set of control tests with the smooth concrete surface. The friction factor of k -type roughness varies with the pitch ratio and becomes maximum around $\lambda/k = 7$ in the absence of a free surface (Leonardi *et al.*, 2003). The four configurations cover the critical range of roughness conditions as well as a large pitch ratio of 20 that corresponds to negligible interactions of the turbulence between roughness elements.

2.2 Instrumentation and Measurements

The flow regime required two types of measuring devices. Resistance-type wire gauges give accurate readings of the surface elevation of non-breaking waves, whereas ultrasonic wave gauges can track sheet flows over dry beds as well as turbulent bores with air entrainment and spray. Fourteen resistance-type wave gauges with parallel wires and seven sonic wave gauges measure the surface wave elevation along the flume with a sampling rate of 50 Hz. Each wave gauge was mounted at a distance of 0.44 m from the side wall. Table 2 lists the installed gauges and their locations from the wave maker. WG1 was placed in front of the reef to measure the incident wave height. WG2 to WG5 and SW1 record the initial shoaling processes of the wave on the slope, while WG6 to WG9 and SW2 record the final shoaling and breaking processes. WG10 to WG14 and SW3 to SW7 capture bore formation and propagation on the reef flat. Both types of gauges were calibrated using a standard method, which relates the water-level variation to the voltage response, before and after each set of tests to ensure linearity and stability.

Because of the relatively steep slope, the incident wave increases in height rapidly and the wave front becomes vertical just prior to wave breaking. The wave gauges at relatively large intervals might not precisely capture the initial breaking wave height.

Simultaneously a video camera captures images of the breaking waves at 30 fps over a $0.5 \text{ m} \times 0.5 \text{ m}$ grid painted on the flume wall. Initiation of wave breaking is defined at the moment when the wave front becomes near vertical just before spilling or jet formation at the crest (Grilli *et al.*, 1996; Hsiao *et al.* 2008). Post-processing of the video images identifies the wave breaking initiation and the wave breaker type. Figure 6 shows a video image of a breaking wave from which the height and depth can be determined.

Table 3 summarizes the test conditions. Experiments were conducted at water depths of 2.36, 2.46, 2.56, and 2.66 m from the bottom of the tank, which correspond to 0, 0.1, 0.2, and 0.3 m of water over the reef flat, and wave height to depth ratios of 0.1 to 0.5. The wave maker generates the prescribed solitary wave with a piston motion. However, energy is lost during the generation process and the resulting wave height is 1 to 2% less than the prescribed value. The incident wave height is thus defined by wave gauge 1 at $x = 17.6 \text{ m}$. Figure 7 shows a photo of a wave before breaking and the correspondent raw data recorded at wave gauge 1. Figure 8 shows the recorded free surface elevations at wave gauge 1 for wave height to depth ratios of 0.1 and 0.5. The different trials produce the same solitary wave profiles despite the initial energy loss demonstrating the precision and repeatability of the wave maker. The trailing waves in Figure 8b are typical for large solitary waves with strong nonlinearity.

The roughness elements were placed on either the reef slope or flat in separate experiments to investigate their effects on shoaling, breaking, and bore formation. The experiments included a series of control tests without the bed-form roughness to provide data for reference and comparison. This results in a total of 746 tests in the three-month laboratory study. Each test provides time series of the surface elevation at the gauges along the flume and videos images of the breaking wave near the reef edge. Additional

post-processing with a weighted-average filter was necessary to remove spikes and outliers from the signals of the sonic wave gauges.

3. NUMERICAL MODEL

A numerical model is used to assist interpretation of the laboratory data and provide a reference for comparison. The energetic wave breaking and bore formation, however, are challenging to numerical models commonly used in coastal engineering design and flood hazard assessment. These shock-related hydraulic processes must satisfy conservation laws across flow discontinuities. This has motivated the development of shock-capturing Boussinesq-type models to describe general coastal processes (e.g., Madsen *et al.*, 2006; Kim *et al.* 2009; Tonelli and Petti 2010; Roeber *et al.* 2010; Dutykh *et al.* 2011; Roeber and Cheung, 2012; Shi *et al.* 2012). These shock-capturing models utilize a Riemann solver to approximate breaking waves as bores and provide good agreement with laboratory experiments. In particular, Roeber and Cheung (2012) re-formulated Nwogu's (1993) Boussinesq-type equations in the conservative form of the nonlinear shallow-water equations and derived a Godunov-type finite volume scheme for the numerical solution. They validated their model with the laboratory data of Roeber (2010) and Swigler and Lynett (2012) as well as field data collected over a fringing reef on Oahu.

The shock-capturing Boussinesq-type model of Roeber and Cheung (2012) provides a useful tool to describe wave transformation processes in fringing reef environments and a future test bed to examine the implementation of additional algorithm to account for the effects of the bed-form roughness. The depth-integrated governing equations, which define the conservation of volume and momentum and in the present one-dimensional problem, read

$$H_t + (Hu)_x + \left[\left(\frac{z_\alpha^2}{2} - \frac{h^2}{6} \right) hu_{.xx} + \left(z_\alpha + \frac{h}{2} \right) h(hU)_{.xx} \right]_x = 0 \quad (1)$$

$$\begin{aligned}
& (Hu)_t + \left(Hu^2 + \frac{1}{2} gH^2 \right)_x - gHh_x \\
& + H \left[z_\alpha \left(\frac{z_\alpha}{2} u_{xx} + (hu_t)_{xx} \right) + \tau \right] \\
& + u \left[\left(\frac{z_\alpha^2}{2} - \frac{h^2}{6} \right) hu_{xx} + \left(z_\alpha + \frac{h}{2} \right) h(hu)_{xx} \right]_x = 0
\end{aligned} \tag{2}$$

where g is acceleration due to gravity, $H = (\eta+h)$ is the flow depth, u is the flow velocity, z_α is a reference depth, and τ is the bed shear stress, parameterized in terms of the Manning coefficient. The governing equations contain the conservative form of the nonlinear shallow-water equations to capture shock-related hydraulic processes. The finite volume method with a Godunov-type scheme and a TVD (Total Variation Diminishing) reconstruction procedure provides a conservative numerical procedure compatible with the governing equations. Time integration of the governing equations evaluates the conserved variables, which in turn provide the horizontal velocity through a linear system of equations derived from the dispersion terms in the momentum equations.

A Riemann solver in the model approximates breaking waves as hydraulic jumps or bores without the use of a predefined mechanism or coefficient. Although the model cannot account for overturning of the free surface, it correctly reproduces the energy dissipation in the wave breaking process through the Riemann solver. The bed shear stress, however, involves the Manning number n empirically related to the bed roughness, and is given by

$$\tau = -n^2 \frac{g}{H^{1/3}} \frac{U \sqrt{U^2 + V^2}}{\rho H} \tag{3}$$

where ρ is water density. A Manning number of $n = 0.014$ describes the smooth concrete finish of the reef model in the control tests. This approach provides a reasonable account for the energy dissipation when a well-defined boundary layer is developed over the

bottom, but is not applicable for bed-form roughness, which modifies the mean flow over the entire water column.

4. RESULTS AND DISCUSSION

The laboratory experiments provided a large volume of time series data for post-processing and analysis. Figures 9 and 10 show, for example, the recorded time series of the free surface elevation from the control tests with plain concrete surface for $H_o/h_o = 0.1$ and 0.5 and $h_f = 0.2$ m. Figure 11 and 12 compare the measured and computed wave profiles along the flume. The input solitary wave, which has a symmetric profile, shoals on the slope with reflection and steepening of the wave until a vertical front face develops and a plunging wave breaker occurs at the reef edge. The wave breaker subsequently transforms into a turbulent bore on the shallow water over the reef flat with continuing energy dissipation. The Boussinesq model of Roeber *et al.* (2010) provides a reasonable description of the wave transformation processes, but slightly underestimates the breaking wave height for the energetic test with $H_o/h_o = 0.5$. The presence of bed forms modifies these processes to varying extents. The recorded data is divided into three sets, which are evaluated for the effects of bed-form roughness on wave shoaling on the slope, breaking near the reef edge, and bore propagation on the flat.

4.1. Wave Shoaling

The shoaling process for a prescribed slope depends on the water depth and wave height as well as on the bed-form roughness. Figs. 13 to 16 show the surface elevation envelopes over the reef slope for the range of water depth from 0 to 0.3 m over the reef flat. Since the slope is uniform, an increasing water depth simply shifts the shoaling process toward the reef flat. An exception occurs at the reef edge, where the shoaling process is interrupted and the wave height depends on the water depth over the reef flat. The bottom conditions show a clear effect on the wave amplitude as the wave shoals and breaks on the slope. An interesting characteristic of solitary waves is that the larger

waves have shorter wavelengths and then thus shoal later, but break earlier on the slope. Little shoaling occurs before wave gauge 3, while the wave height increases almost linearly from wave gauges 3 to 7 prior to wave breaking for all the tests. The recorded data from gauges 3 to 7 allows examination of the effects of bed-form roughness on the shoaling process.

Figure 17 shows the wave height gradient between gauges 3 and 7 as a function of the average height to depth ratio indicative of the local nonlinearity during the shoaling process. The data obtained with the four water depths, which represent different stages of the shoaling process, show a similar pattern with the roughness. The control tests with a smooth concrete bed give the highest wave height gradient. The bedform roughness increases the friction and dissipates wave energy during the shoaling process. The wave height gradient decreases appreciably beyond the margin of laboratory errors. Both the pitch ratio and roughness height influence the dissipation. Over the range of pitch ratios from 5 to 20, BF3 with a value of 10 results in the strongest dissipation and lowest gradient. This is consistent with the finding from Leonardi *et al* (2003) that the friction factor is maximum at an intermediate range of pitch ratios. BF1 has the same pitch ratio of 10, but produces less dissipation because of the lower roughness height.

The celerity, which is the same as group velocity in shallow water, is a good indicator of the shoaling process. Figure 18 shows the measured celerity between gauges 3 and 7 as a function of the bed form and wave height to depth ratio. The data does not show clear effects of the roughness pitch ratio or height on the celerity and its spread is within the range of laboratory errors. The average water depth between gauges 3 to 7 ranges from 165 to 55 cm for the four tests and is large compared to the roughness height of 3.8 and 7.6 cm. The effects the bed-form roughness do not reach far enough into the water column to affect the momentum exchange in the mean flow and the resulting wave

properties. The results in Figures 17 and 18 show that the roughness dissipates energy and reduces the wave height but does not directly modify the celerity during the shoaling process.

4.2. Wave Breaking

Wave breaking occurs between gauges 7 and 9 for most of the tests. The wave height gradient between these two gauges provides a general indication of the roughness effects on the wave breaking process. Figure 19 shows the wave height gradient for the four series of tests with 0 to 0.3 m water depth on the reef flat. The results in general show a downward trend of the gradient with nonlinearity as energetic breaking of the larger waves dissipates more energy. An increasing water depth effectively shifts the smaller breaking waves toward the reef edge at gauge 9 and increases the effects of the standing water over the reef flat on the breaking process. This results in less energy dissipation or even some effects of shoaling between gauges 7 and 9 for the smaller waves and accounts for the initial upward trend and positive values of the gradient in $h_f = 0.2$ and 0.3 m.

The results show a clear influence of the bottom roughness in the wave breaking process. The smooth bed tests yield the highest gradient or lowest energy dissipation rate as expected. The energy dissipation shows much stronger dependence on the pitch ratio than roughness height. BF2 with the lowest pitch ratio of 5 shows the highest dissipation rate among all the tests, while BF4 with the largest pitch ratio of 20 produce very similar results as the control test with a smooth bed. BF1 and 3, which have the same pitch ratio of 10, produce very similar results despite their different roughness heights. In contrast to wave shoaling, a smaller pitch ratio of 5 appears to correspond to the highest friction factor in the surf zone. This is likely due to the reduced water depth at the wave breaker that allows interactions between the turbulence generated by wave breaking and the

bedform roughness. It was observed during the experiments that the bedform roughness causes the wave to start breaking in deeper water and increases the length of the surf zone. This increases the dissipation rate and shifts the data points in Figure 19 toward the left and bottom for all four tests with bed-form roughness.

Analysis of the videos taken during the experiment provides the location of the wave breaker. Figure 20 shows clear relations between the breaking water depth and the incident wave height and bed roughness. The results from $h_f = 0$ and 10 cm give the same linear relation between the breaking water depth and incident wave height. As the water depth increases, the smaller waves break at the reef edge resulting in a constant breaking water depth. The remaining results from $h_f = 0.2$ m show very similar relations with the incident wave height, while the larger water depth of $h_f = 0.3$ m on the reef flat influences the breaking water depth even on the reef slope. The measurements confirm the observations that the bed roughness causes the waves to break earlier. The breaking depth increases with the roughness height and with decreasing pitch ratios. The closely spaced and tall roughness elements decrease the effective water depth for wave propagation forcing the waves to break further offshore. However, the increase in breaking depth varies with the incident wave height reaching an average value of 9.2 cm for $H_o/h_o \geq 0.45$. This is considerably larger than the corresponding roughness height of 7.6 cm and suggests a second mechanism associated with the roughness elements in the wave breaking process. The roughness elements redirect the predominantly horizontal flow upward and introduce velocity perturbation that may lead to earlier breaking. Numerical model results of solitary wave propagation on bed-form roughness show transfer of momentum from the bottom to the free surface causing acceleration of the wave crest just prior to wave breaking (Nar Sambe *et al.* 2011).

Despite the energy dissipation during shoaling and the larger breaking depth, the breaking wave height in Figure 21 does not show significant effects of the bedform roughness. There appears to be a balance between energy dissipation and upward momentum transfer from the bedform roughness. The breaking index, which is defined as the ratio of the breaking wave height and depth, is an important parameter in surf-zone processes. Figure 22 shows the breaking index as a function of the incident wave height and bed-form roughness. The results include only the waves that break on the slope for consistency. Because of the steep slope, the waves break in shallower water. This results in a large breaking index of 1.5 to 5.5 for small waves and 2.5 to 4 for large waves. The small waves break closer to the reef edge. The influence from the standing water on the reef flat is obvious and accounts for the wider range of breaking indices. These values are high compared to 1.36 to 1.47 reported by Grilli *et al.* (1997) with the same criteria for numerically generated breaking waves on a gentle beach slope of 1:35. The breaking index decreases with increasing roughness height as the waves break in deeper water while the breaking wave height remains essentially unchanged. The pitch ratio appears to play a secondary role with effects in the range of laboratory errors.

4.3. Bore Propagation

The timber and strut setup was transferred from the reef slope to the flat in the second phase of the laboratory study. The breaking wave at the reef edge transforms into a bore over the reef flat for examination of dissipation and propagation over bed-form roughness. Figures 23 to 25 plot the bore height along the flat from gauges 9 to 14 for the three tests with water depths of 0.1 to 0.3 m on the reef flat. The bore height decreases along the flat due to dissipation from turbulence and bottom friction as well as attenuation of the input flow at the reef edge over time. The smooth bed gives the largest bore height and the lowest rate of reduction to provide a reference for comparison. The bed-form roughness

increases the dissipation rate and its effect is more significant with decreasing water depth.

Fig. 26 plot the wave height gradient between gauges 9 and 14 as a function of the input bore height to illustrate the dissipation across the reef flat. The gradient shows a clear relation with the input bore height and roughness height. The dissipation rate increases with the input bore height due to more energetic wave breaking and turbulence at the bore front as well as the shorter wavelength of the larger incident solitary wave. The results show strong dependence on the roughness height, because of the direct relation between the form drag on the roughness element and the bottom friction. A higher pitch ratio contributes to minor reduction of the gradient, but the effect is negligible compared with that of the roughness height. Since the roughness height is of the same order as the water depth, the turbulence extends to the free surface regardless of the element spacing. This is important for numerical modeling of wave transformation over fringing reefs as the roughness pitch ratio is often poorly defined. The roughness height is the key parameter in defining the wave friction factor in fringing flat reef environment as already demonstrated by Filipot and Cheung (2012).

The bore speed is an important characteristic parameter in shock propagation. The bore is unsteady near the reef edge from the initial breaking process and becomes better defined at wave gauge 12. Figure 27 shows the average celerity between wave gauges 12 and 14 as a function of the relative bore height in the three tests. The results show the bed-form roughness plays a significant role in bore propagation on the reef flat. When the bore height and flow depth are small, the bed form trend to decrease the bore speed. Observations during the experiments show the roughness elements generate an undulating bore, which has a smaller propagation speed. As the flow depth increases with the bore height, the undulation diminishes at the surface. The changes in propagations

speed can be attributed in part to a decrease in effective depth associated with the presence of bed forms and the reduction in the near-bed flow. This increases the bore speed according to the Riemann solution for shock propagation (Mohamed, 2008). The roughness elements may also enhance vertical advection that increases the flow speed near the surface as shown in the numerical results of Nar Sambe et al. (2011). A higher pitch ratio with more widely spaced roughness elements reduces their effect on the free surface flow. The overall effect also diminishes with increasing water depth and the results from the different bed forms appear to converge to the control test with the smooth bed.

5. CONCLUSIONS AND RECOMENDATIONS

A series of large-scale laboratory experiments have provided a unique dataset to elucidate wave shoaling, breaking, and bore propagation over bed-form roughness on an idealized fringing reef. The use of solitary wave in the experiments allows precise measurements of wave transformation across the reef without interference from return flows or wave setup. Construction of the bed form by timber beams facilitates a systematic approach to investigate its effects in terms of the roughness height and pitch ratio. The experiments utilized the k -type roughness, which generates turbulence into the water column, to better mimic the effects of coral reefs. A set of control tests with the smooth concrete surface provide a reference for comparison. The wave transformation processes were recorded by resistance and sonic wave gauges along the flume as well as a video system for post-processing.

The bed-form roughness increases the bottom friction and dissipates wave energy during the shoaling process. For the small roughness height compared to the water depth, the bed form does not modify the wave propagation characteristics appreciably. The measurements are able to reproduce a previous finding that the highest dissipation rate occurs at an intermediate range of pitch ratios. As the water depth decreases relative to the roughness height, a smaller pitch ratio produces the highest dissipation rate at wave breaking. The bed form reduces the effective water depth for wave propagation and increases the vertical advection and the surface velocity. The breaking depth increases with the roughness height and decreasing pitch ratio, while the breaking wave height remains largely unaffected. The roughness height is the key parameter defining the bore propagation and dissipation rate on the reef flat. The celerity of the smaller waves decreases because of formulation of undular bores over the bed form, while the bed form speeds up the larger bores because of vertical advection.

The experiments have produced a unique dataset for calibration of numerical models to reproduce effects of bed-form roughness in modeling of coastal wave transformation. The recorded dissipation rates on the reef slope and flat can be readily used to calibrate the wave friction factor and the eddy viscosity for phase-averaged and phase-resolving models. Existing parameterizations, however, are insufficient to account for the bed-form effects on wave breaking and bore propagation. These sub-grid features modify intrinsic wave properties in addition to the dissipation rate. It is necessary to develop new parameterizations that enhance vertical advection in a multi-layer model to describe acceleration of the surface flow, formulation of undular bore, and modification of the bore speed. Additional experiments on a wider range of roughness heights and pitch ratios as well as current measurements will certainly help to produce a comprehensive dataset for model calibration.

REFERENCES

- Chen, D., Chen, C., Tang, F.-E., Stansby, P., and Li, M. (2007). Boundary layer structure of oscillatory open-channel shallow flows over smooth and rough beds. *Experiments in Fluids*, 42(5), 719-736.
- Dixen, M., Hatipoglu, F., Sumer, B.M., and Fredsøe, J. (2008). Wave boundary layer over a stone-covered bed. *Coastal Engineering*, 55(1), 1-20.
- Dutykh, D., Katsaounis, T., and Mitsotakis, D. (2011). Finite volume schemes for dispersive wave propagation and runoff. *Journal of Computational Physics*, 230(8), 3035-3061.
- Filipot, J.F., and Cheung, K.F. (2012). Spectral wave modeling in fringing reef environments. *Coastal Engineering*, 67, 67-79.
- Fuhrman, D.R., Fredsøe, J., and Sumer, B.M. (2009). Bed slope effects on turbulent wave boundary layers: 1. Model validation and quantification of rough-turbulent results. *Journal of Geophysical Research*, 114(C3), 1-16.
- Furuya, Y., Miyata, M., and Fujita, H. (1976). Turbulent Boundary Layer and Flow Resistance on Plates Roughened by Wires. *Journal of Fluids Engineering*, 76, 635-644.
- Gerritsen, F. (1981). Wave Attenuation and Wave Set-up on a Coastal Reef. PhD Dissertation, University of Trondheim, Norway.
- Grilli, S.T., Subramanya, R., Svendsen, I.A., and Veeramony, J. (1994). Shoaling of Solitary Waves on Plane Beaches. *Journal of Waterway, Port, Coastal and Ocean Engineering*, 120(6), 609-628.
- Grilli, S.T., Svendsen, I.A., and Subramanya, R. (1997). Breaking Criterion and Characteristics for Solitary Waves on Slopes. *Journal of Waterway, Port, Coastal and Ocean Engineering*, 123(3), 102-112.
- Hardy, T.A., and Young, I.R. (1996). Field study of wave attenuation on an offshore coral reef. *Journal of Geophysical Research*, 101(C6), 14311-14326.
- Hsiao, S.-C., Hsu, T.-W., Lin, T.-C., and Chang, Y.-H. (2008). On the evolution and run-up of breaking solitary waves on a mild sloping beach. *Coastal Engineering*, 55(12), 975-988.
- Kim, D.-H., Lynett, P.J., and Socolofsky, S.A. (2009). A depth-integrated model for weakly dispersive, turbulent, and rotational fluid flows. *Ocean Modelling*, 27(3-4), 198-214.

- Leonardi, S., Orlandi, P., Smalley, R.J., Djenidi, L., and Antonia, R.A. (2003). Direct numerical simulations of turbulent channel flow with transverse square bars on one wall. *Journal of Fluid Mechanics*, 491, 229-238.
- Li, Y., and Raichlen, F. (2001). Solitary wave runup on plane slopes. *Journal of Waterway, Port, Coastal and Ocean Engineering*, 127(1), 33-44.
- Liu, P.L.-F., Park, Y.S., Cowen, E.A. (2007). Boundary layer flow and bed shear stress under a solitary wave. *Journal of Fluid Mechanics*, 574, 449-463.
- Lowe, R.J., Falter, J.L., Bandet, M. D., Pawlak, G., Atkinson, M.J., Monismith, S.G., and Koseff, J.R. (2005). Spectral wave dissipation over a barrier reef. *Journal of Geophysical Research*, 110(C4), 1-16.
- Lowe, R.J., Hart, C., and Pattiaratchi, C.B. (2010). Morphological constraints to wave-driven circulation in coastal reef-lagoon systems: A numerical study. *Journal of Geophysical Research*, 115(C9), 1-13.
- Lowe, R.J., Shavit, U., Falter, J.L., Koseff, J.R., and Monismith, S.G. (2008). Modeling flow in coral communities with and without waves : A synthesis of porous media and canopy flow approaches. *Limnology and Oceanography*, 53(6), 2668-2680.
- Madsen, P.A., Fuhrman, D.R., and Wang, B. (2006). A Boussinesq-type method for fully nonlinear waves interacting with a rapidly varying bathymetry. *Coastal Engineering*, 53(5-6), 487-504.
- Mirfenderesk, H., and Young, I.R. (2003). Direct measurements of the bottom friction factor beneath surface gravity waves. *Applied Ocean Research*, 25(5), 269-287.
- Mohamed, A. (2008). Characterization of Tsunami-like Bores in Support of Loading on Structures. MS Thesis, University of Hawaii, Honolu.
- Nar Sambe, A., Golay, F., Sous, D., Fraunie, P., Rey, V., Marcel, R., Jouette, C.D., Principia, R., and Ciotat, L. (2011). Two-phase-flow unstructured grid solver: application to tsunami wave impact. *International Journal of Offshore and Polar Engineering*, 21(3), 186-191.
- Nelson, R.C. (1996). Hydraulic roughness of coral reef platforms. *Applied Ocean Research*, 18(5), 265-274.
- Nunes, V. and Pawlak, G. (2008). Observations of bed roughness of a coral reef. *Journal of Coastal Research*, 24(2B), 39-50.
- Nwogu, O. (1993). Alternative form of Boussinesq equations for nearshore wave propagation. *Journal of Waterway, Port, Coastal and Ocean Engineering*, 119(6), 618-638.

- Ojha, S.P., and Mazumder, B. S. (2010). Turbulence characteristics of flow over a series of 2-D bed forms in the presence of surface waves. *Journal of Geophysical Research*, 115(F4), 1-15.
- Raudkivi, A.J. (1988). The roughness height under waves. *Journal of Hydraulic Research*, 26(5), 569-584.
- Roeber, V. (2010). Boussinesq-Type Model for Nearshore Wave Processes in Fringing Reef Environment. PhD Dissertation, University of Hawaii, Honolulu.
- Roeber, V., and Cheung, K.F. (2012). Boussinesq-type model for energetic breaking waves in fringing reef environment. *Coastal Engineering*, in press.
- Roeber, V., Cheung, K.F., and Kobayashi, M.H. (2010). Shock-capturing Boussinesq-type model for nearshore wave processes. *Coastal Engineering*, 57(4), 407-423.
- Shi, F., Kirby, J.T., Harris, J.C., Geiman, J.D., and Grilli, S.T. (2012). A high-order adaptive time-stepping TVD solver for Boussinesq modeling of breaking waves and coastal inundation. *Ocean Modelling*, 43-44, 36-51.
- Sleath, J.F.A. (1987). Turbulent oscillatory flow over rough beds. *Journal of Fluid Mechanics*, 182, 369-409.
- Suntoyo, and Tanaka, H. (2009). Numerical modeling of boundary layer flows for a solitary wave. *Journal of Hydro-environment Research*, 3(3), 129-137.
- Suntoyo, Tanaka, H., and Sana, A. (2008). Characteristics of turbulent boundary layers over a rough bed under saw-tooth waves and its application to sediment transport. *Coastal Engineering*, 55(12), 1102-1112.
- Swigler, D.T. (2009). Laboratory Study Investigating the Three-Dimensional Turbulence and Kinematic Properties Associated with a Breaking Solitary Wave. MS Thesis, Texas A&M University, College Station.
- Synolakis, C.E. (1987). The runup of solitary waves. *Journal Fluid Mechanics*, 185, 523-545.

Table 1 Sensor Types and Locations

Name	Slope Location (m)	Name	Flat Reef Location (m)
wg1	17.64	wg10	58.05
wg2	28.60	wg11	61.70
wg3	35.91	wg12	65.38
wg4	40.58	wg13	72.72
wg5	44.25	wg14	80.03
wg6	46.1	uswg3	57.88
wg7	48.23	uswg4	61.51
wg8	50.37	uswg5	65.19
wg9	54.41	uswg6	72.5
uswg1	40.58	uswg7	79.84
uswg2	54.41		

Table 2 Bed-form Configurations

Bed Form	Description	k (cm)	λ (cm)	Pitch Ratio (λ/k)
BF1	Small bedform, closely spaced	3.8	38.9	10
BF2	Large bedform, closely spaced	7.6	38.9	5
BF3	Large bedform, widely spaced	7.6	76.9	10
BF4	Small Bedform, widely spaced	3.8	76.9	20
BF0	No bedform, smooth concrete beach and reef	0	0	0

Table 3. Test Conditions

H_o/h_o	H (m)			
	WL0	WL10	WL20	WL30
0.05	0.118	0.123	0.128	0.133
0.1	0.236	0.246	0.256	0.266
0.15	0.354	0.369	0.384	0.399
0.2	0.472	0.492	0.512	0.532
0.25	0.590	0.615	0.640	0.665
0.3	0.708	0.738	0.768	0.798
0.4	0.944	0.984	1.024	1.064
0.45	1.062	1.107	1.152	1.197
0.5	1.180	1.230	1.280	

* Waves were run every 20-30 minutes in order to allow the water to settle.

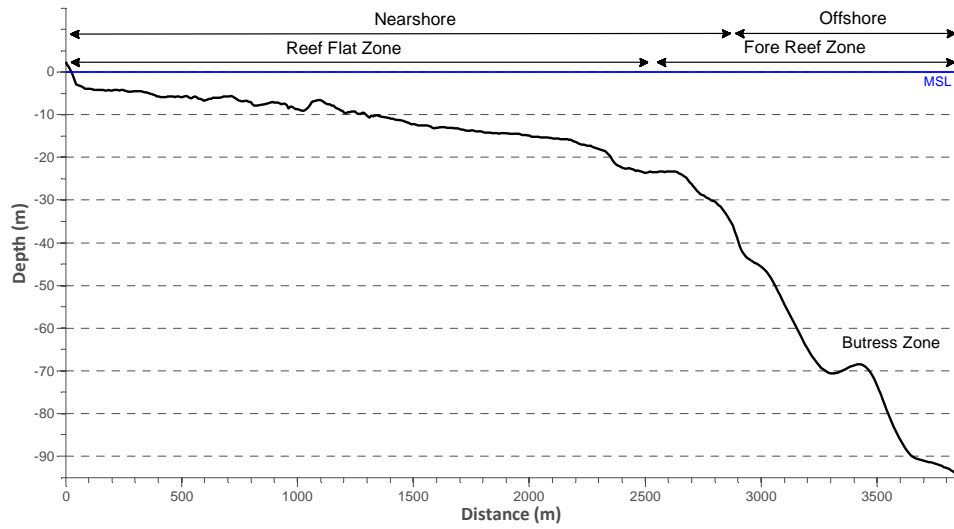


Figure 1. Fringing reef profile at Kailua, Hawaii.

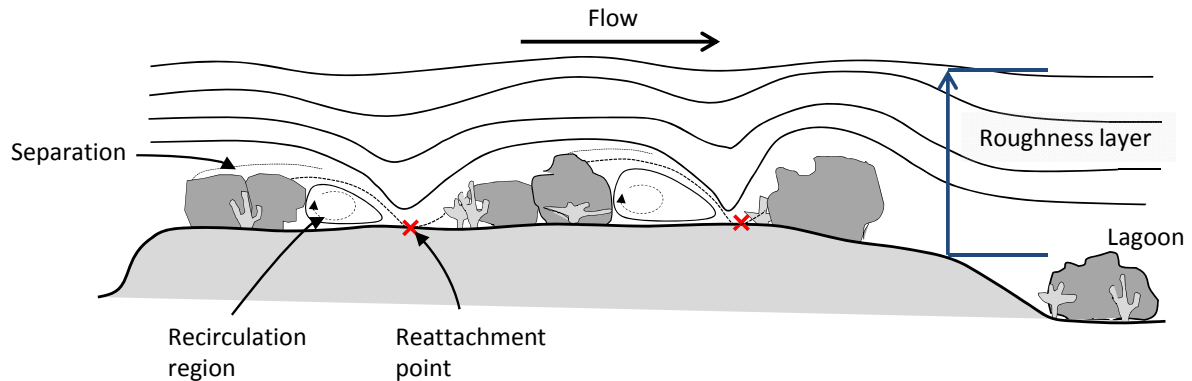


Figure 2. Schematic of free surface flow over roughness elements on fringing reefs.

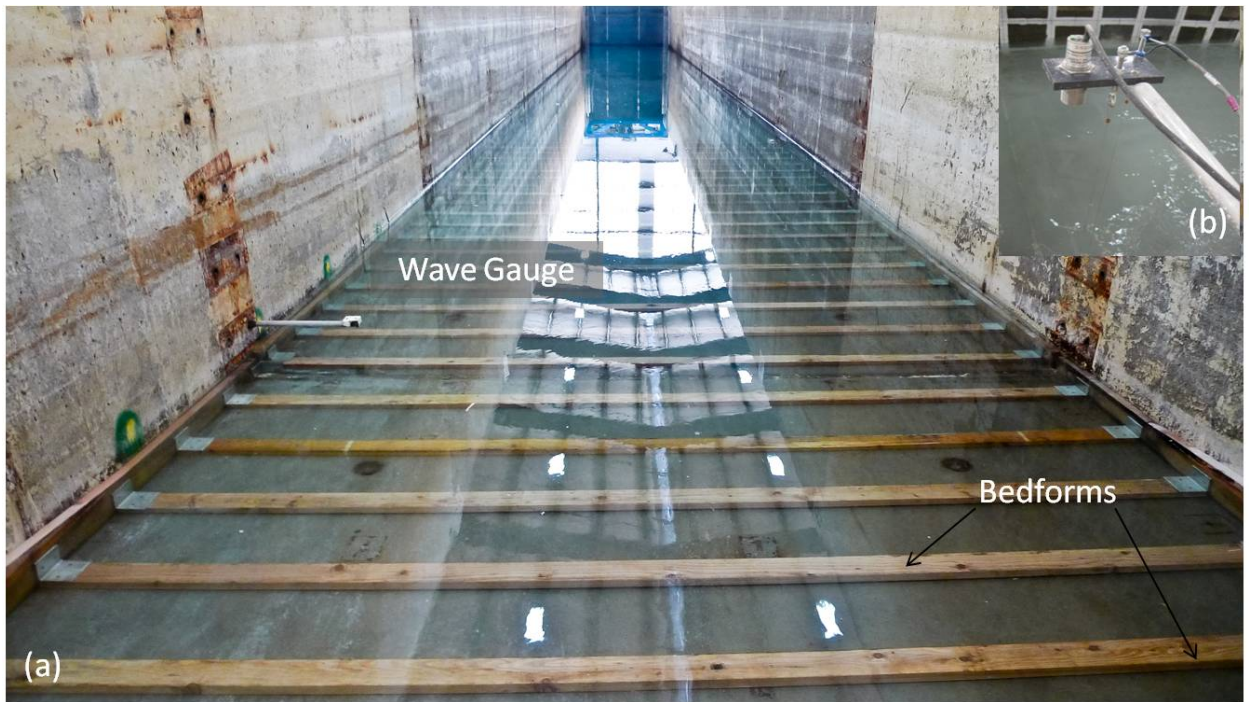


Figure 5. Photo of the installed bed-form roughness and a wired wave gauge. (b) Close-up view of the wire wave gauge.

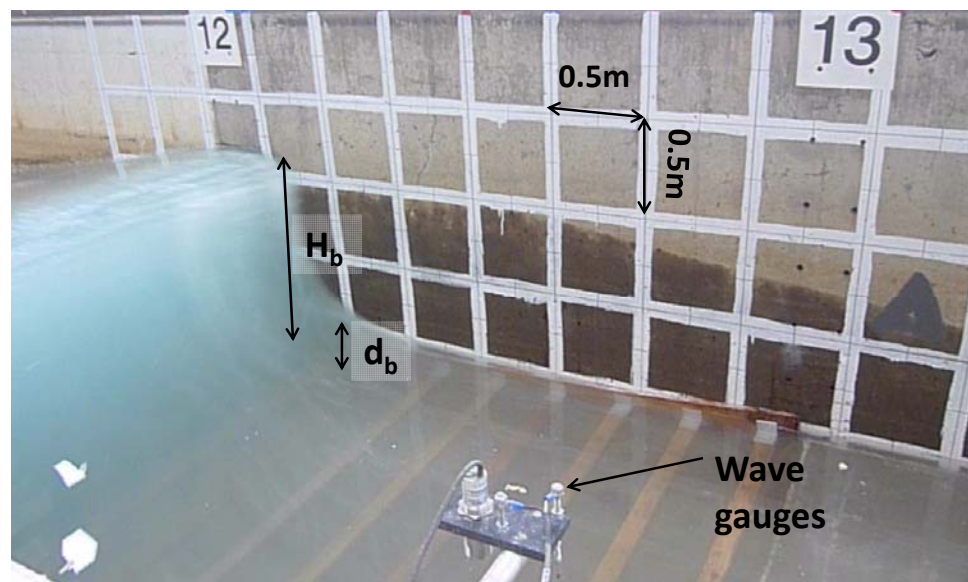


Figure 6. Video capture of a breaking wave and its measurements.

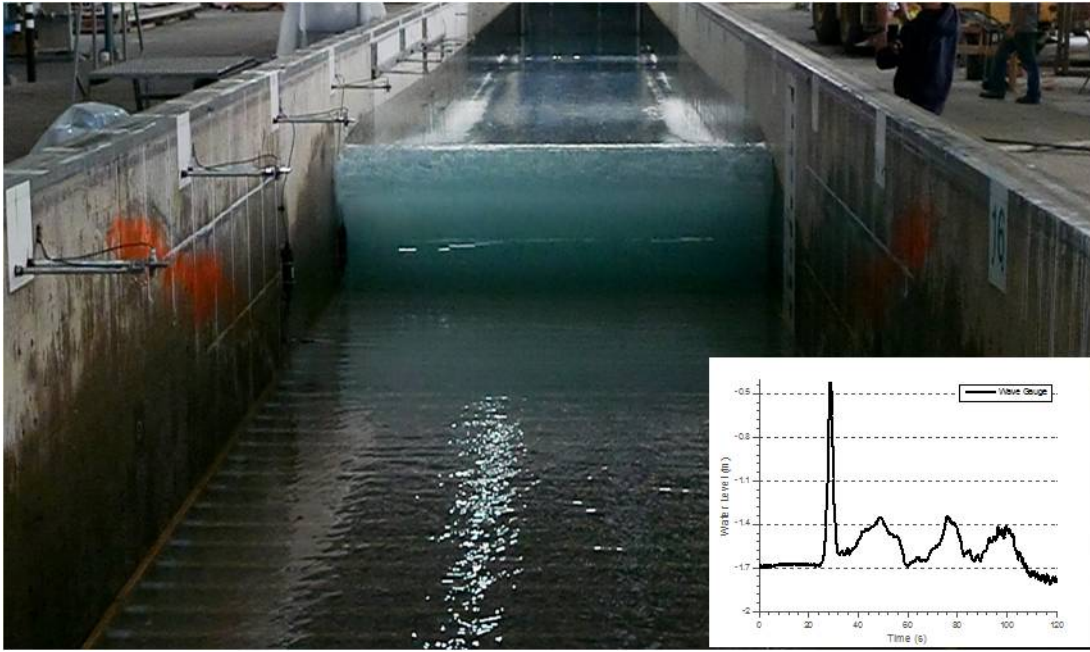


Figure 7. Photo of a solitary wave and the correspondent record at wave gauge 1 ($x = 17.6\text{m}$).

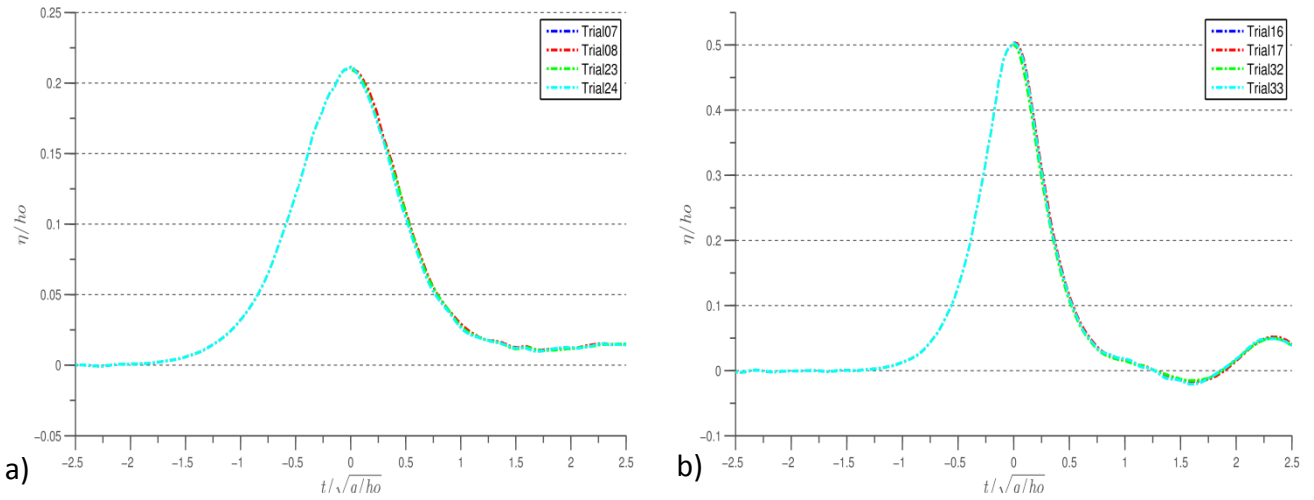


Figure 8. Comparison of recorded surface elevations at wave gauge 1 ($x = 17.6\text{ m}$) from different trials. (a) Trial 7, 8, 23, and 24 for $H_o/h_o = 0.1$ and (b) Trials 16, 17, 32, and 33 for $H_o/h_o = 0.5$.

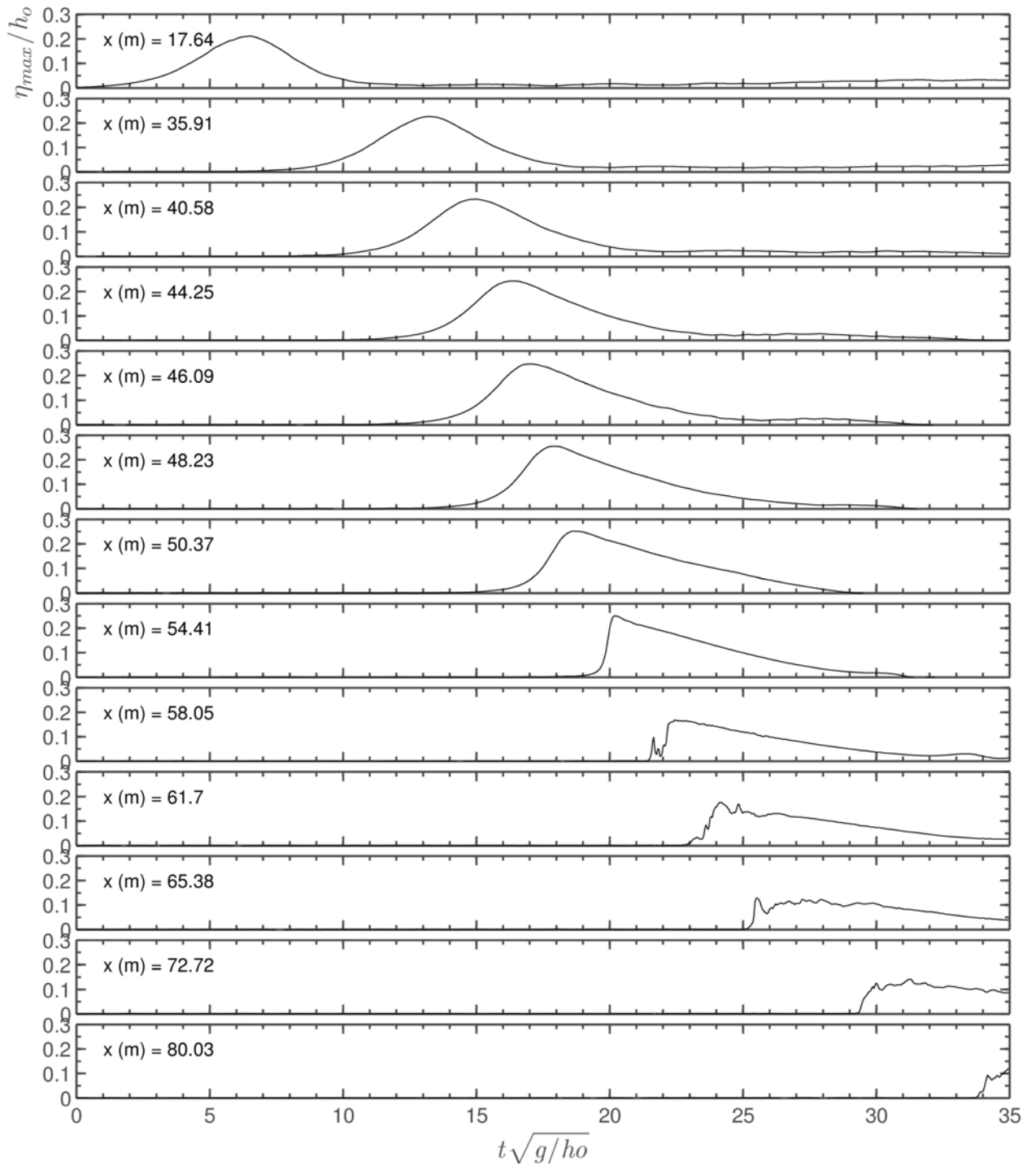


Figure 9. Time series of free surface elevation along the flume at $H_o/h_o = 0.1$ and $h_f = 0.2$ m.

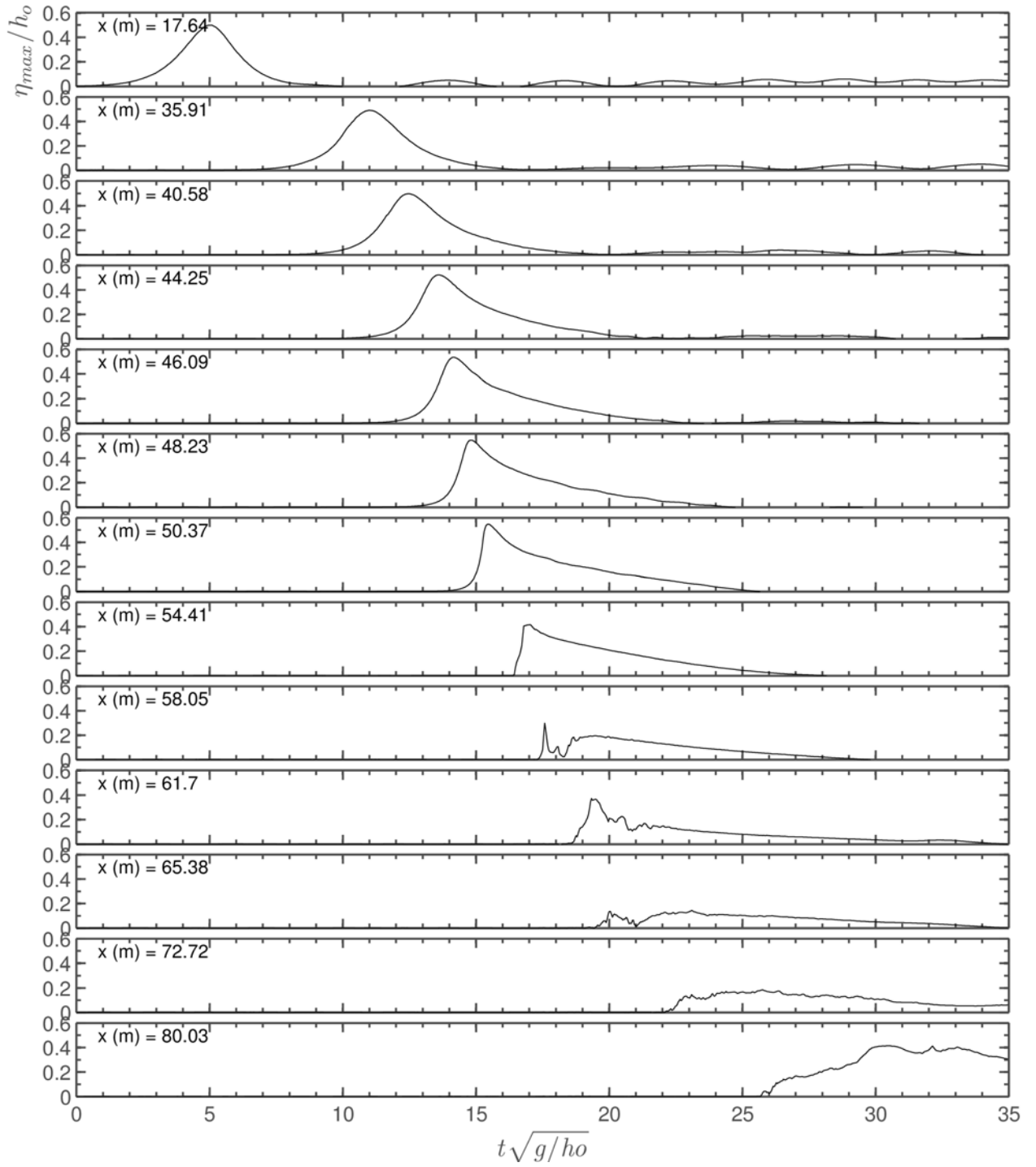


Figure 10. Time series of free surface elevation along the flume at $H_o/h_o = 0.5$ and $h_f = 0.2$ m.

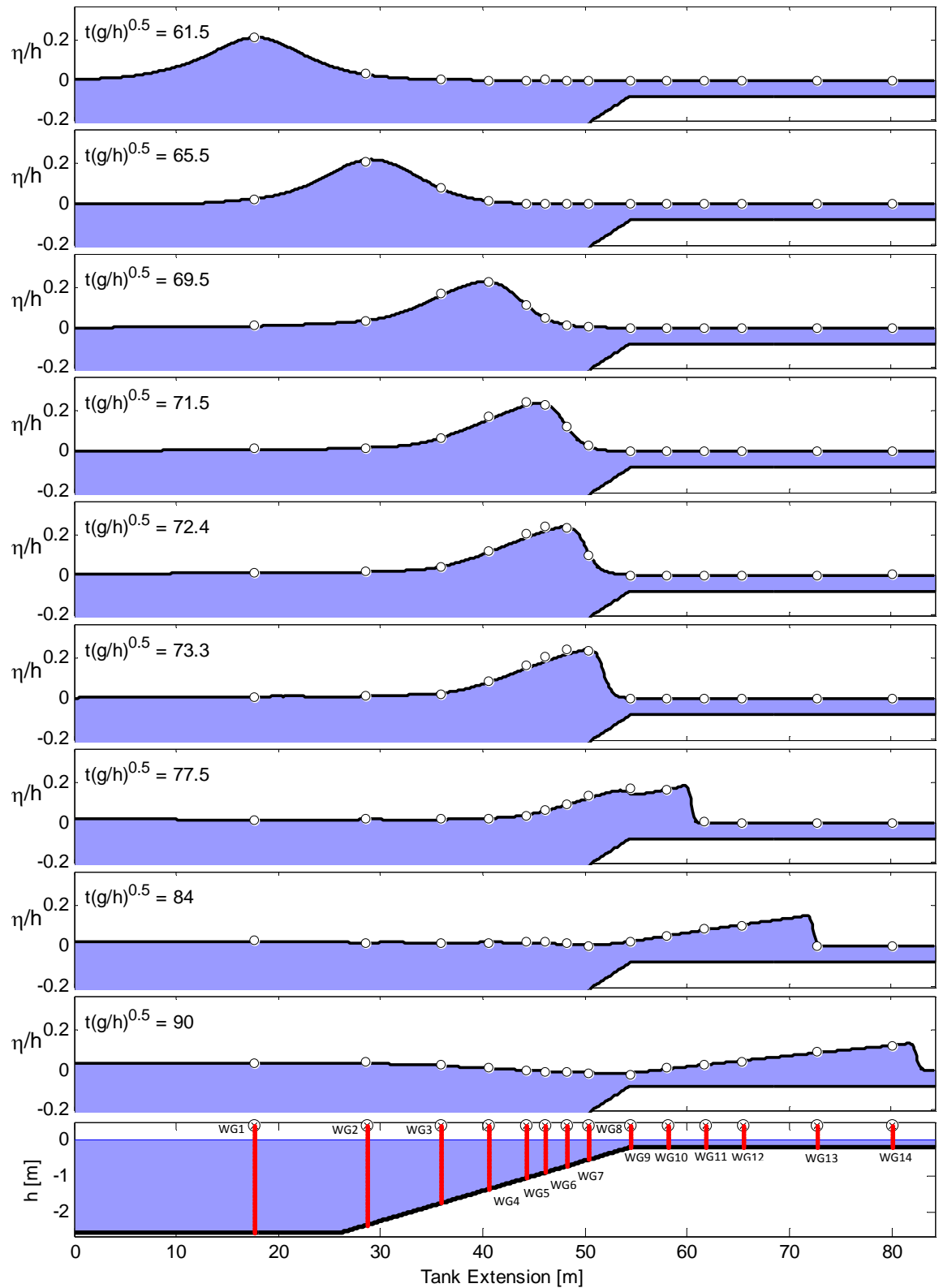


Figure 11. Evolution of computed and recorded free surface profiles at $H_o/h_o = 0.1$.

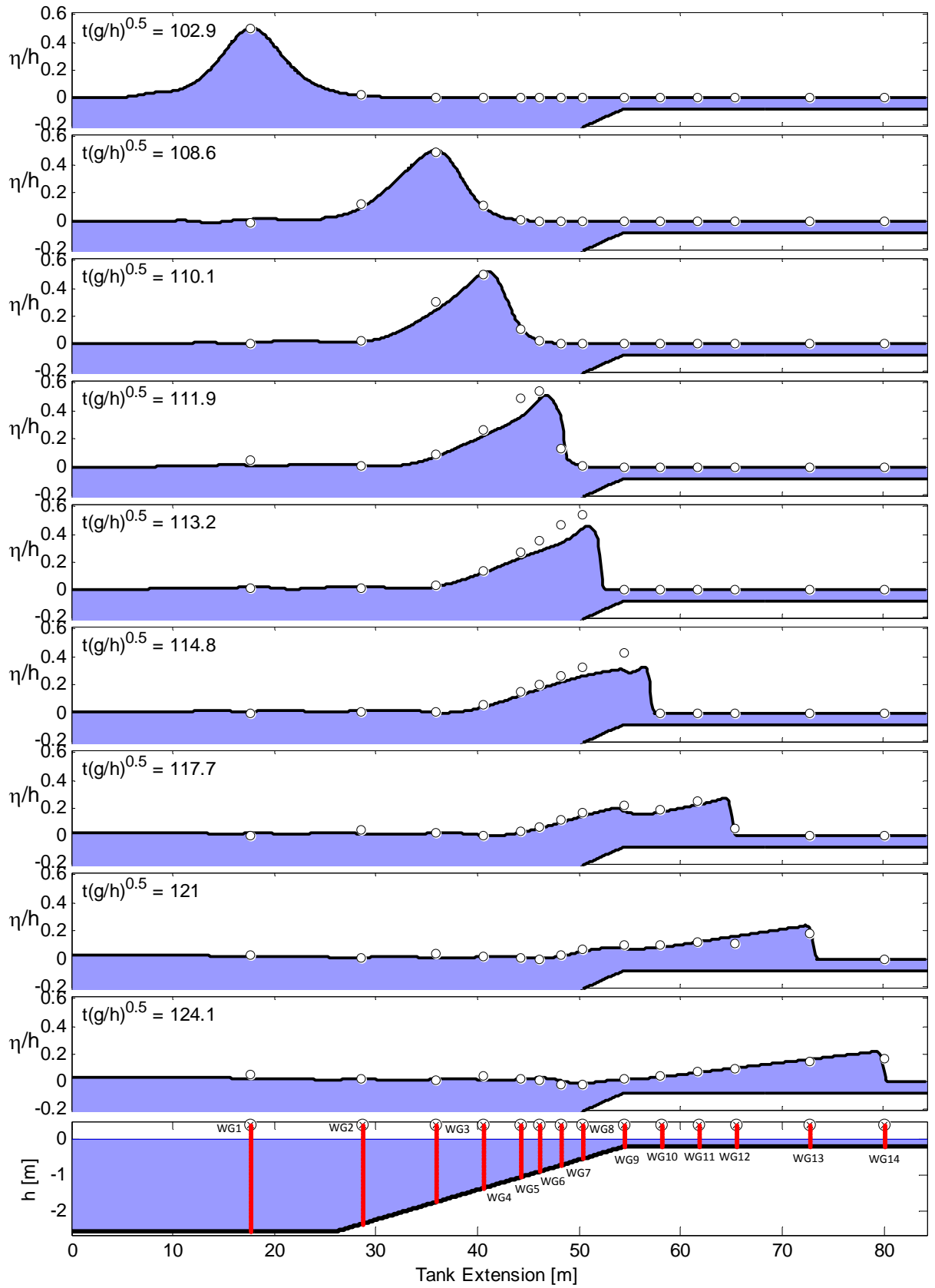


Figure 12. Time history of computed and recorded free surface profiles at $H_o/h_o = 0.5$.

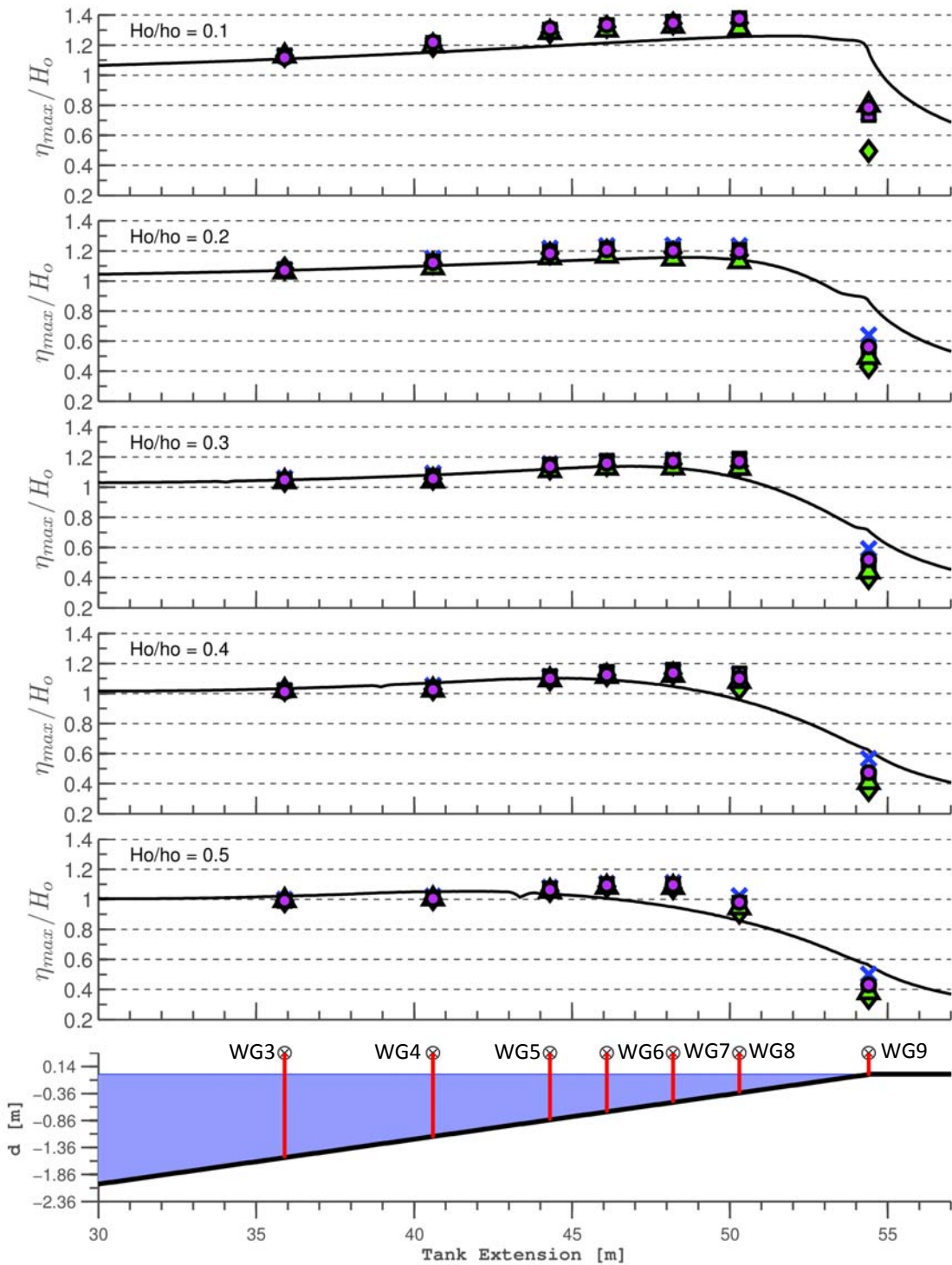


Figure 13. Normalized crest elevation along the reef slope (X BF0, ■ BF1, ◆ BF2, ▲ BF3, ● BF4) and computed solution (- solid line) at 0 cm of water level from the flat reef.

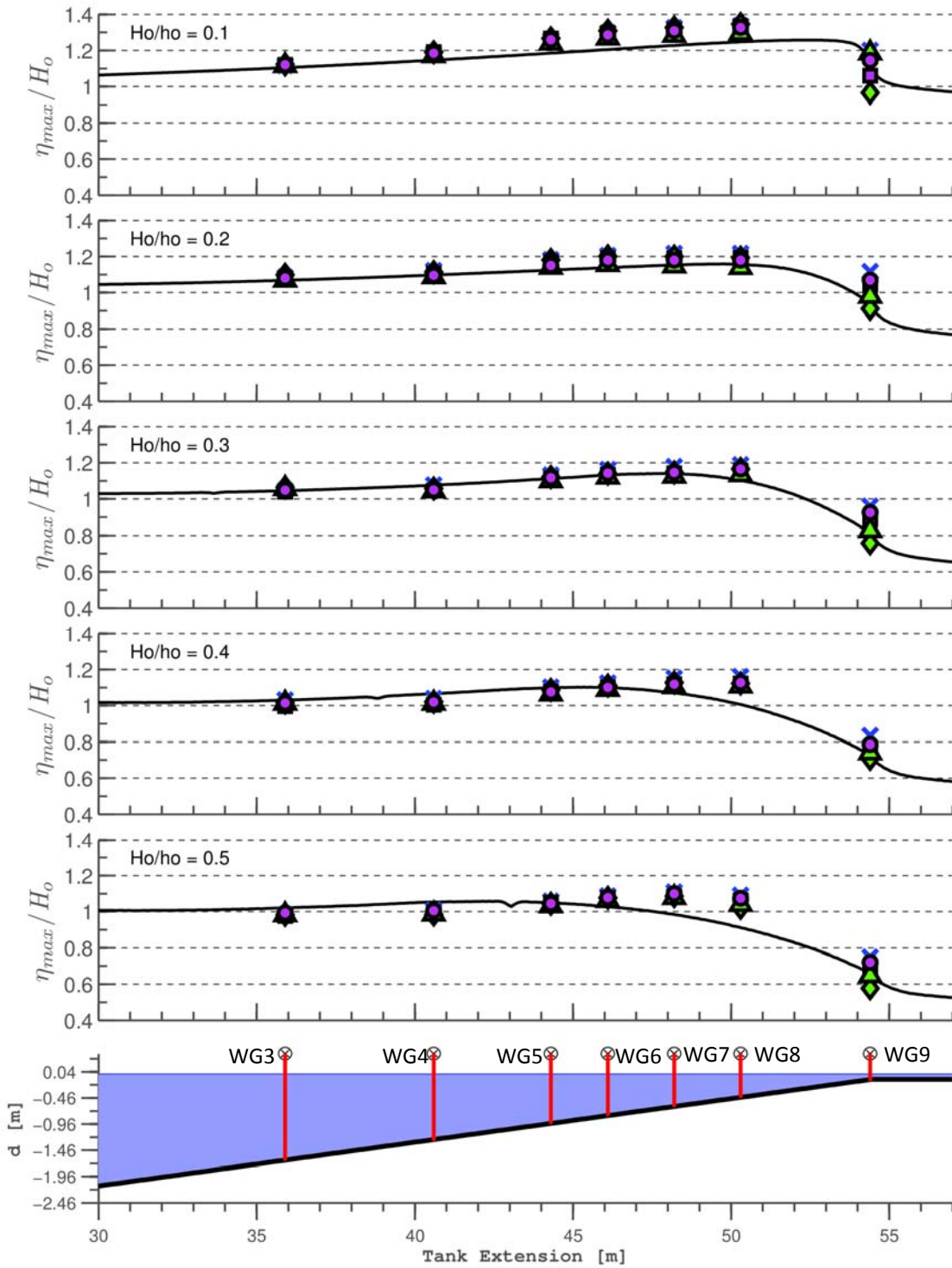


Figure 14. Normalized crest elevation along the reef slope (X BF0, ■ BF1, ◆ BF2, ▲ BF3, ● BF4) and computed solution (- solid line) at 10 cm of water level from the flat reef.

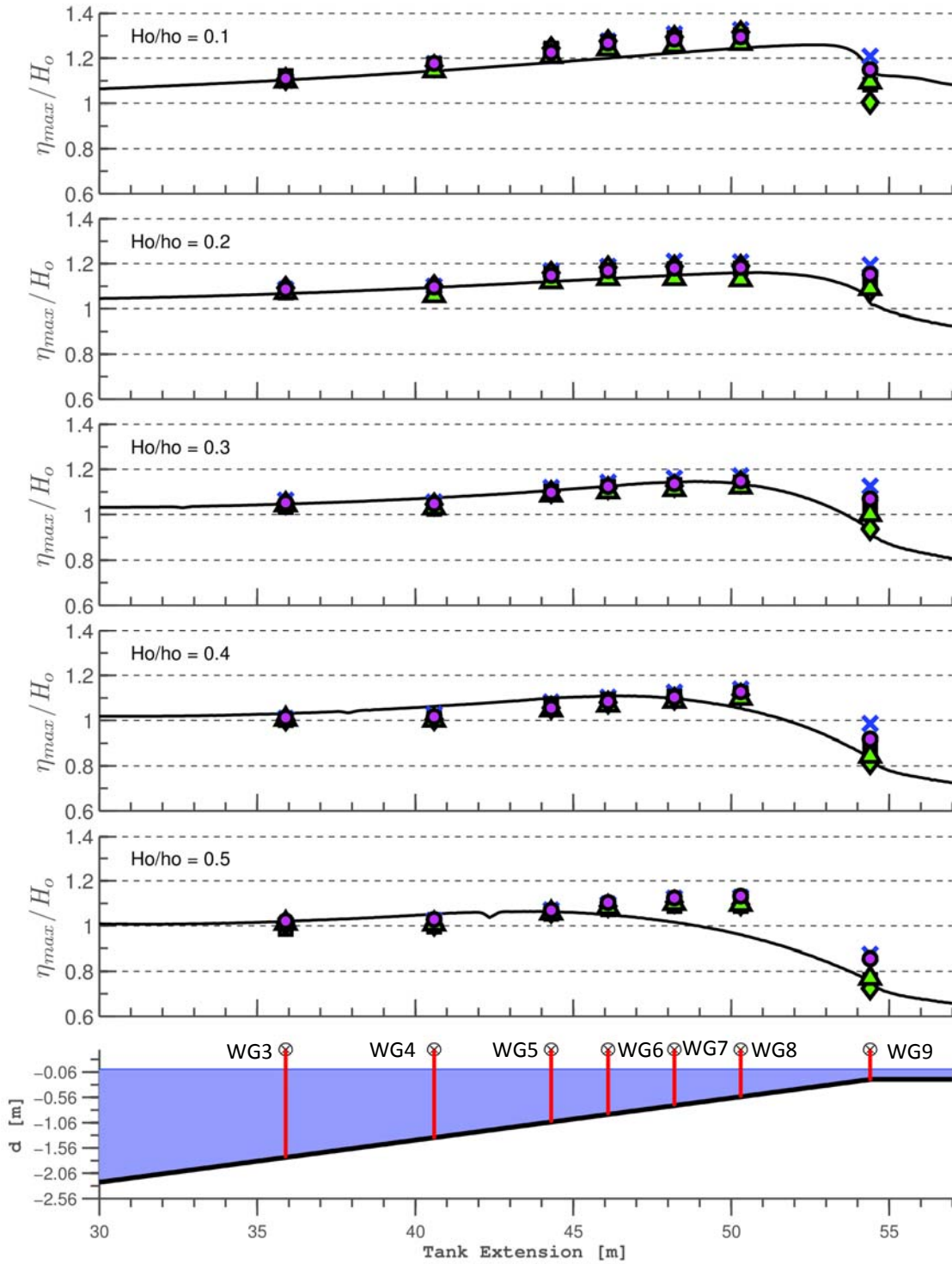


Figure 15. Normalized crest elevation along the reef slope (X BF0, ■ BF1, ◆ BF2, ▲ BF3, ● BF4) and computed solution (- solid line) at 20 cm of water level from the flat reef.

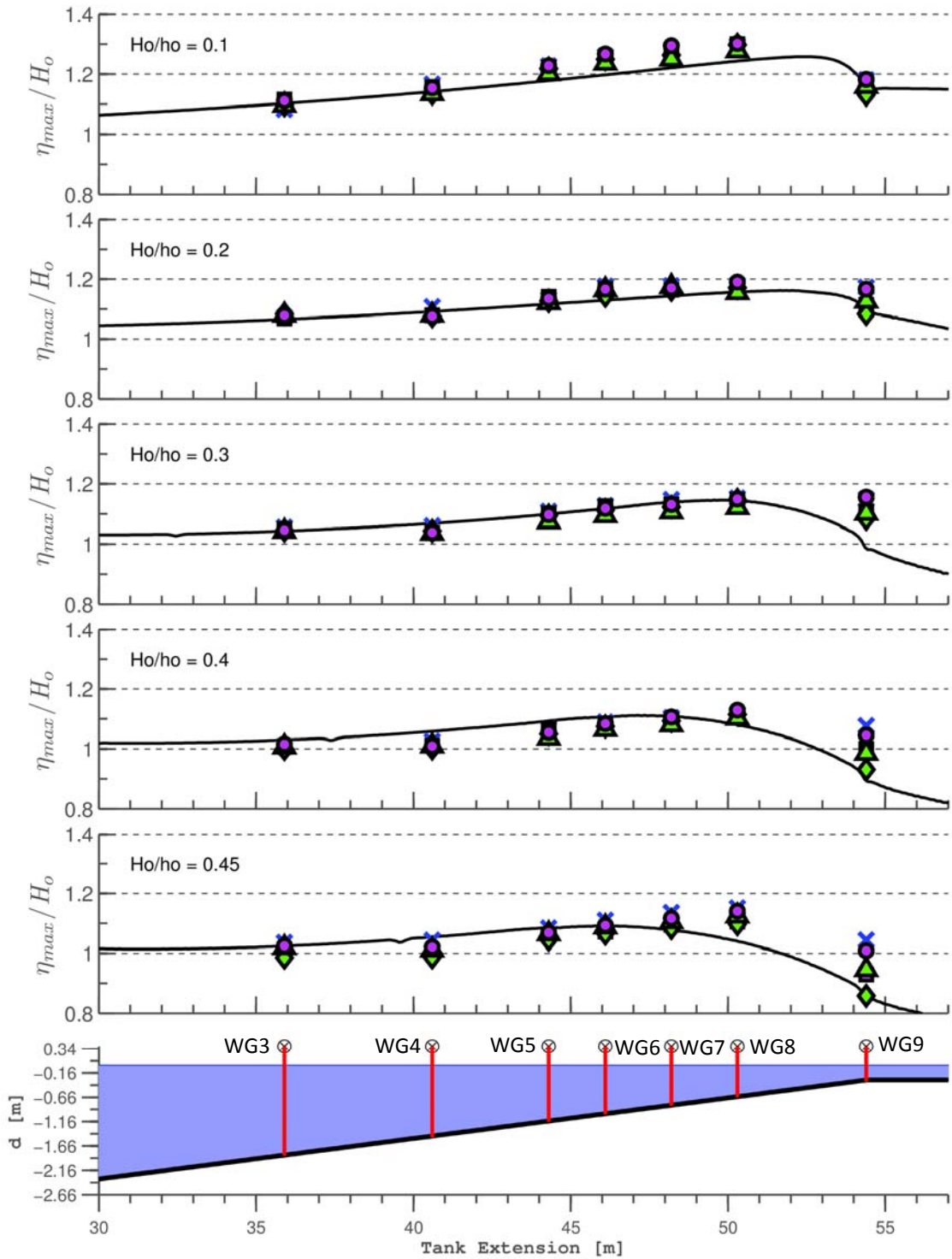


Figure 16 Normalized crest elevation along the reef slope (X BF0, ■ BF1, ◆ BF2, ▲ BF3, ● BF4) and computed solution (- solid line) at 30 cm of water level from the flat reef.

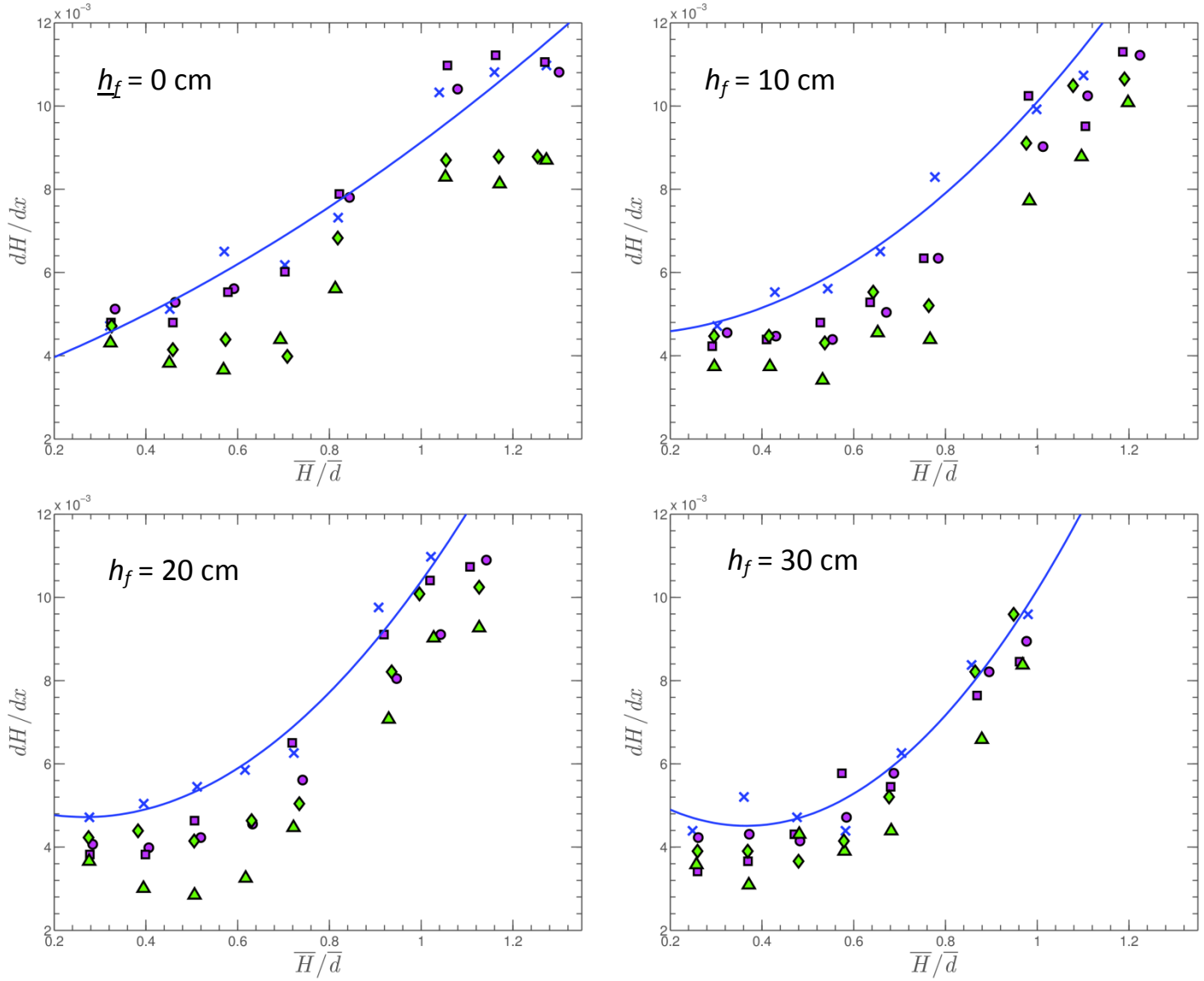


Figure 17. Wave height gradient between wg3 ($x = 35.9$ m) and wg7 ($x = 48.2$ m) on the reef slope (-X- BF0, \blacksquare BF1, \blacklozenge BF2, \blacktriangle BF3, \bullet BF4).

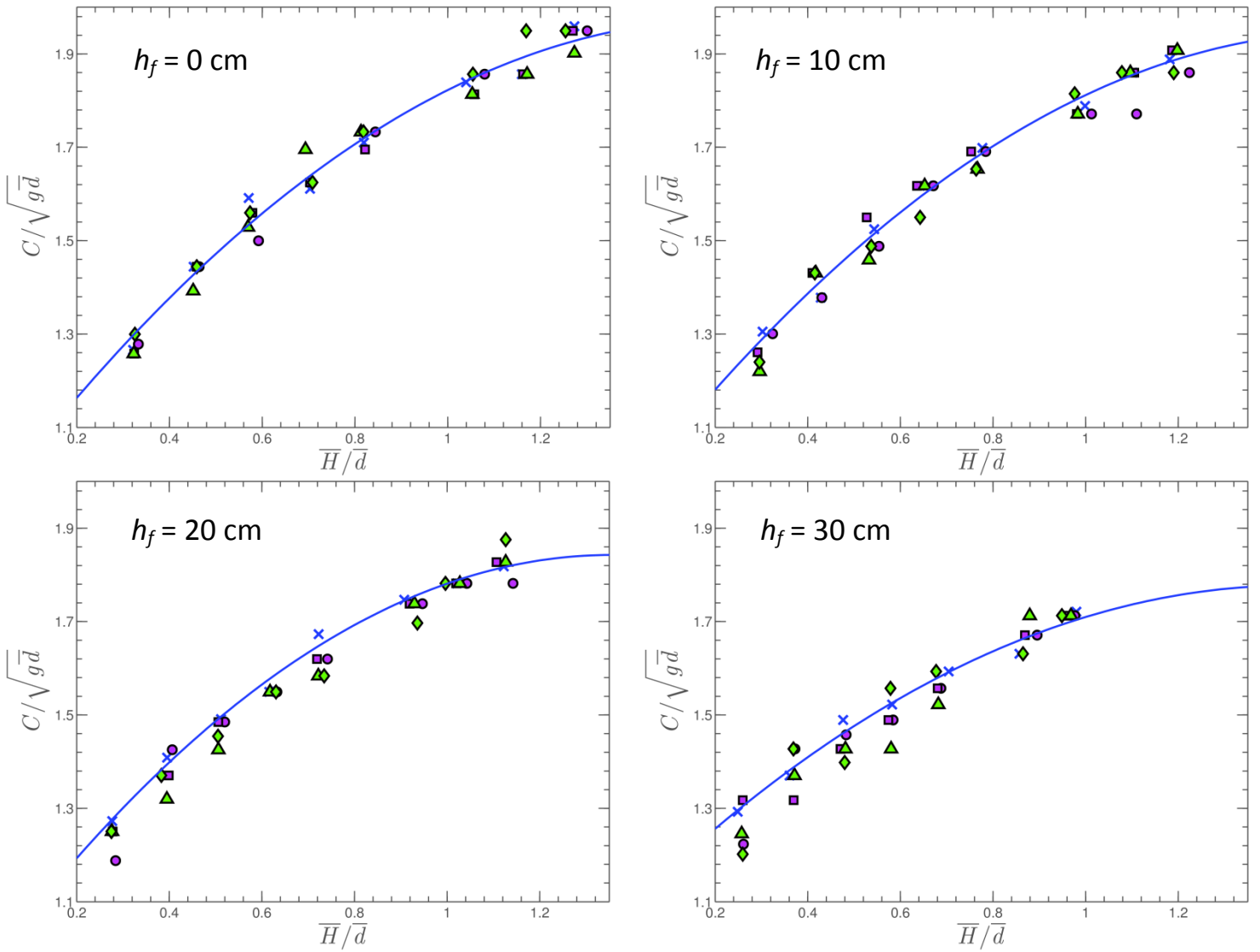


Figure 18. Average celerity between wg3 ($x = 35.9$ m) to wg7 ($x = 48.2$ m) on the reef slope (\times - BF0, \blacksquare BF1, \blacklozenge BF2, \blacktriangle BF3, \bullet BF4).

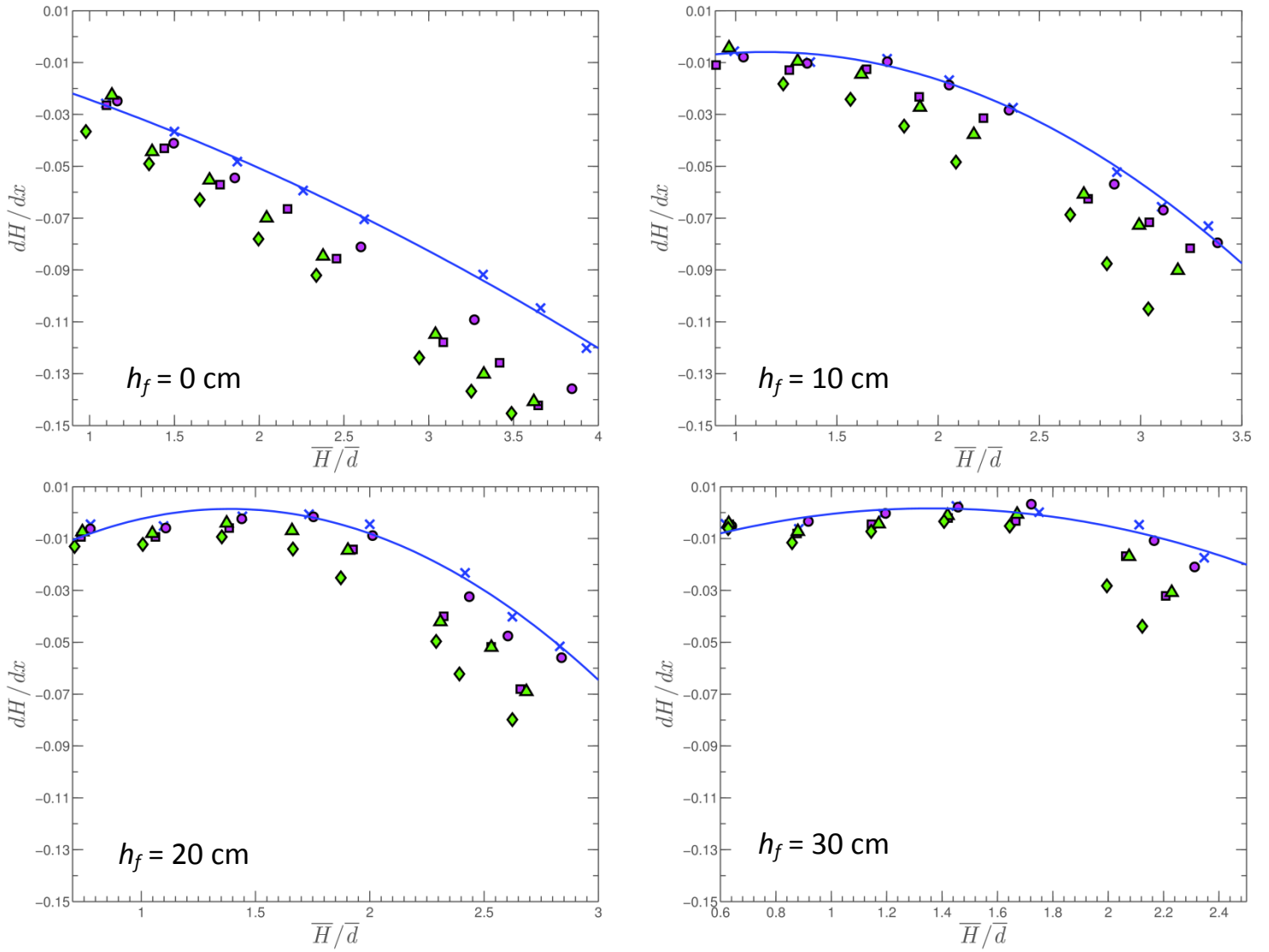


Figure 19. Wave height gradient across the wave breaker between wg7 ($x = 48.2$ m) and wg9 ($x = 54.4$ m) on the reef slope (-X- BF0, \blacksquare BF1, \blacklozenge BF2, \blacktriangle BF3, \bullet BF4).

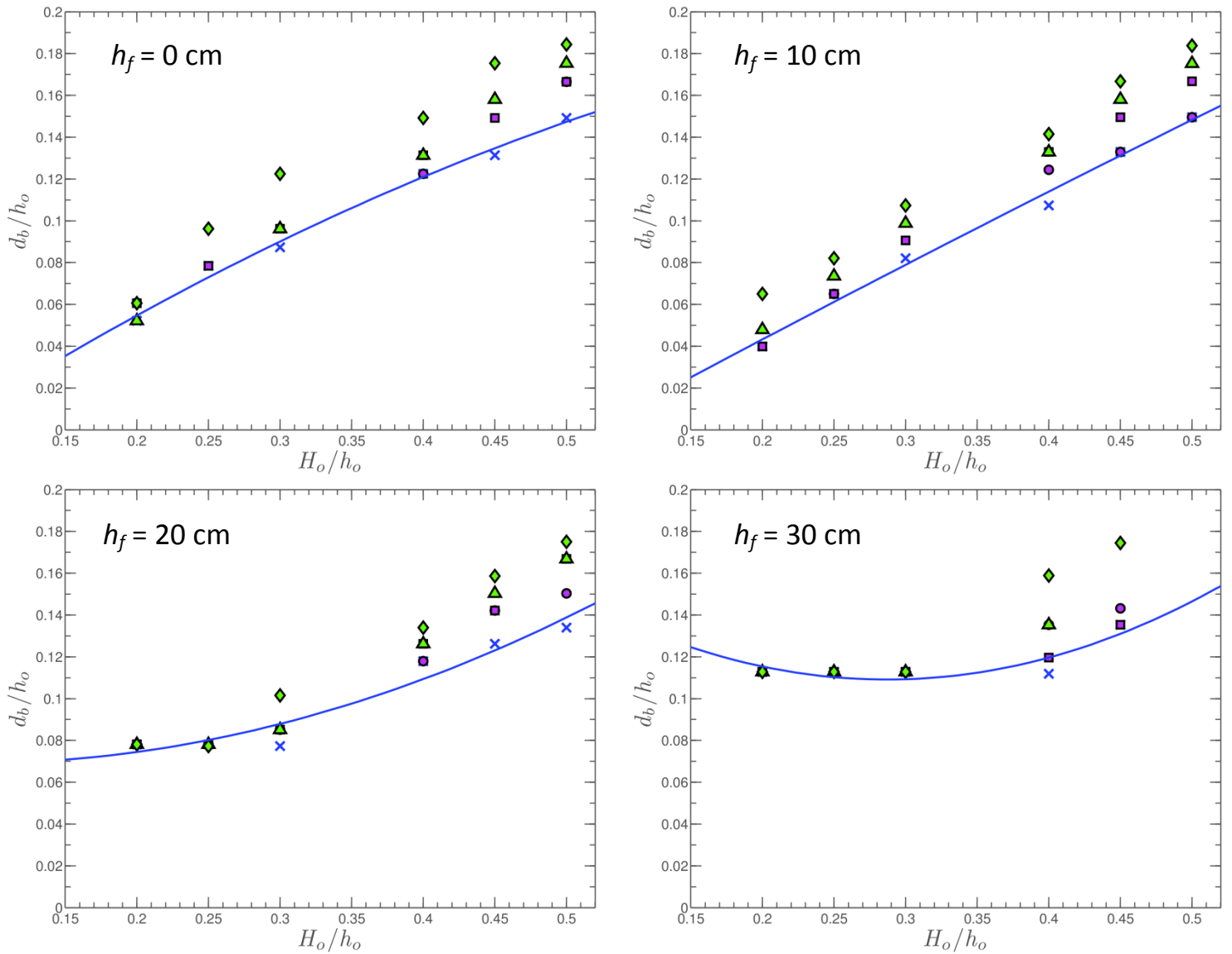


Figure 20. Wave breaking depth on the reef slope (-X- BF0, ■ BF1, ◆ BF2, ▲ BF3, ● BF4).

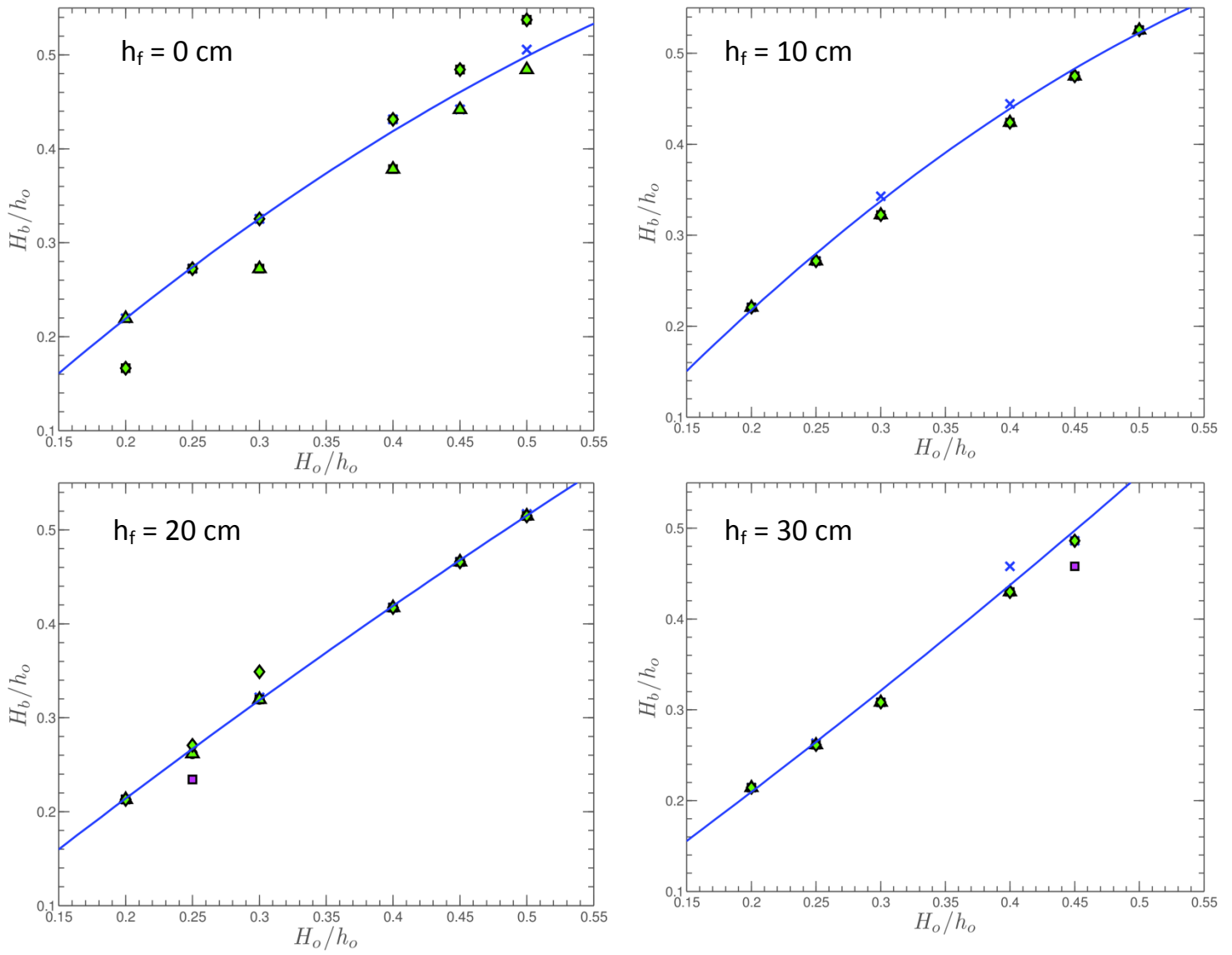


Figure 21 Breaking wave height on the reef slope. (-X- BF0, ■ BF1, ◆ BF2, ▲ BF3, ● BF4).

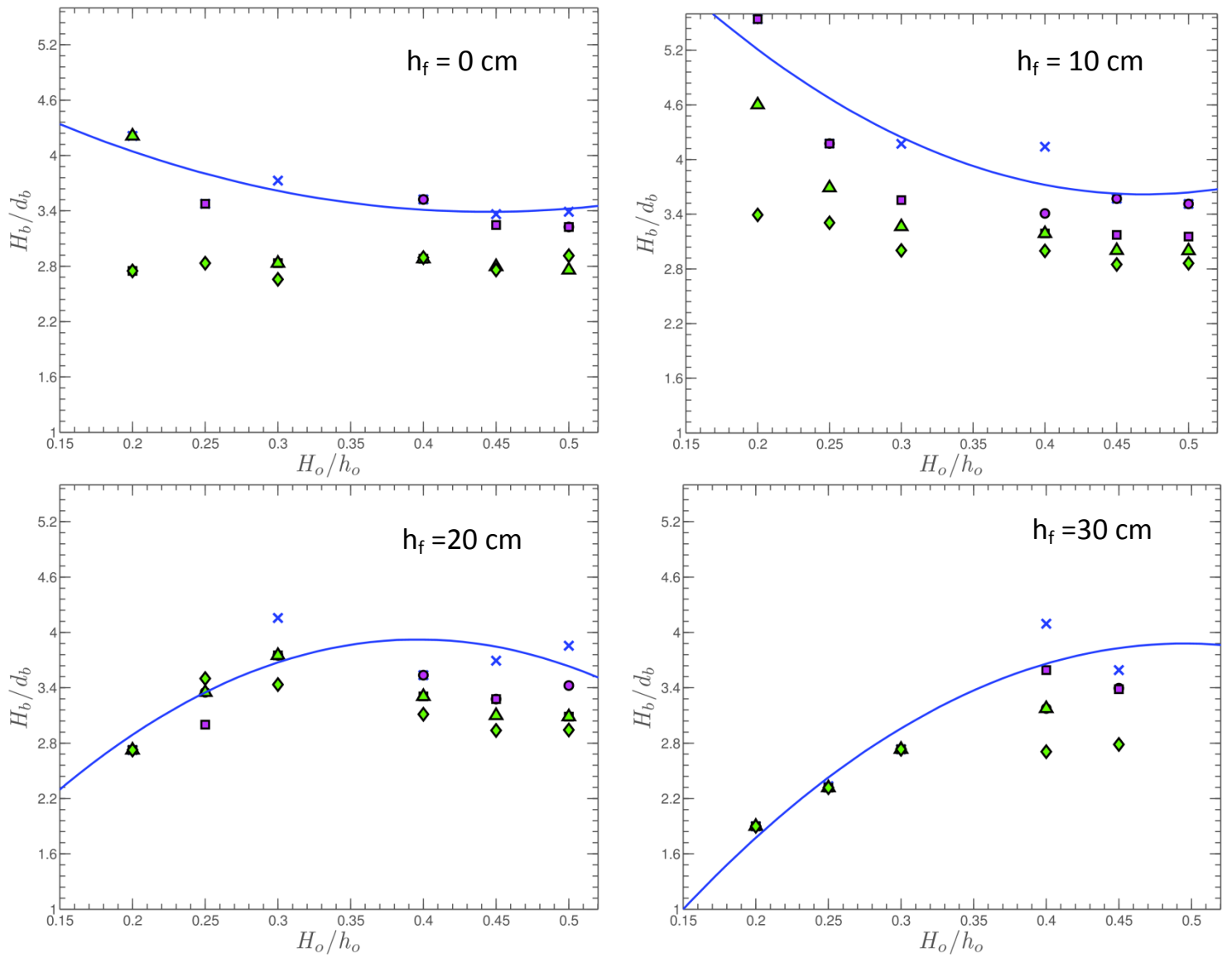


Figure 22. Wave breaking Index (-X- BF0, \blacksquare BF1, \blacklozenge BF2, \blacktriangle BF3, \bullet BF4).

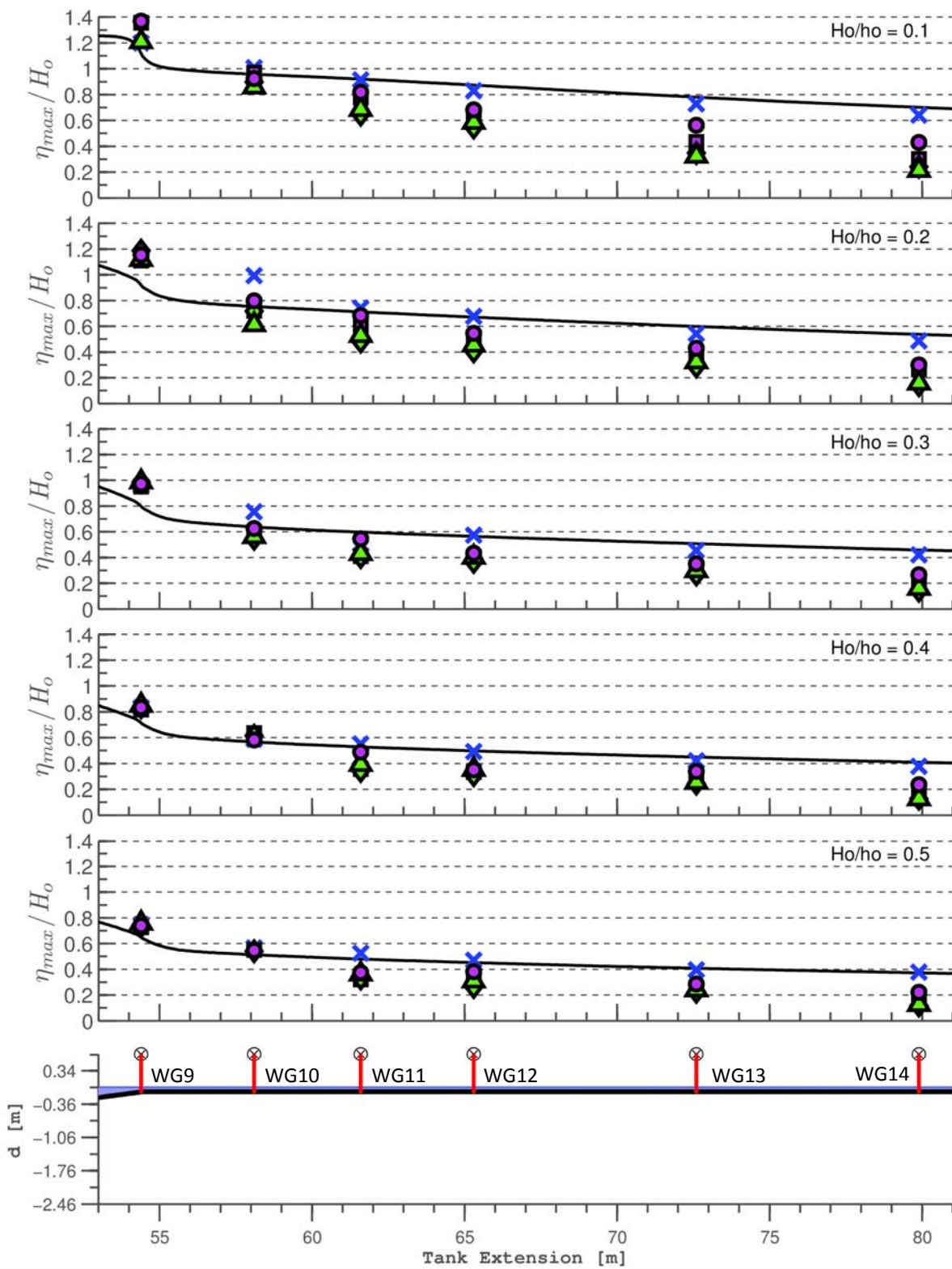


Figure 23. Normalized crest elevation along the flat reef with $h_f = 0.1$ m (-X- BF0, \blacksquare BF1, \blacklozenge BF2, \blacktriangle BF3, \bullet BF4) and computed solution (- solid line) at 10 cm water level from the flat reef.

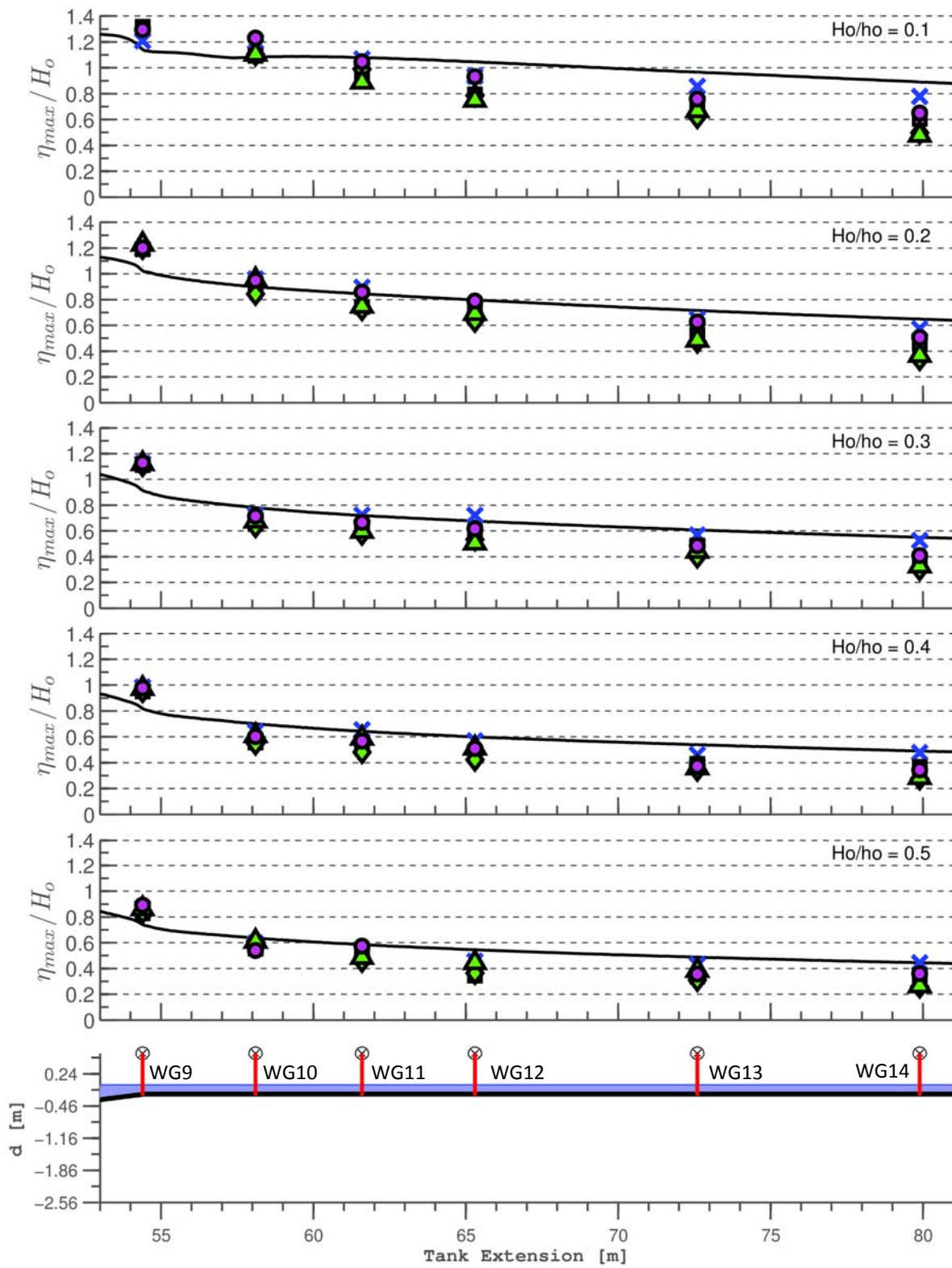


Figure 24. Normalized crest elevation along the flat reef with $h_f = 0.2$ m (-X- BF0, \blacksquare BF1, \blacklozenge BF2, \blacktriangle BF3, \bullet BF4) and computed solution (- solid line) at 20 cm water level from the flat reef.

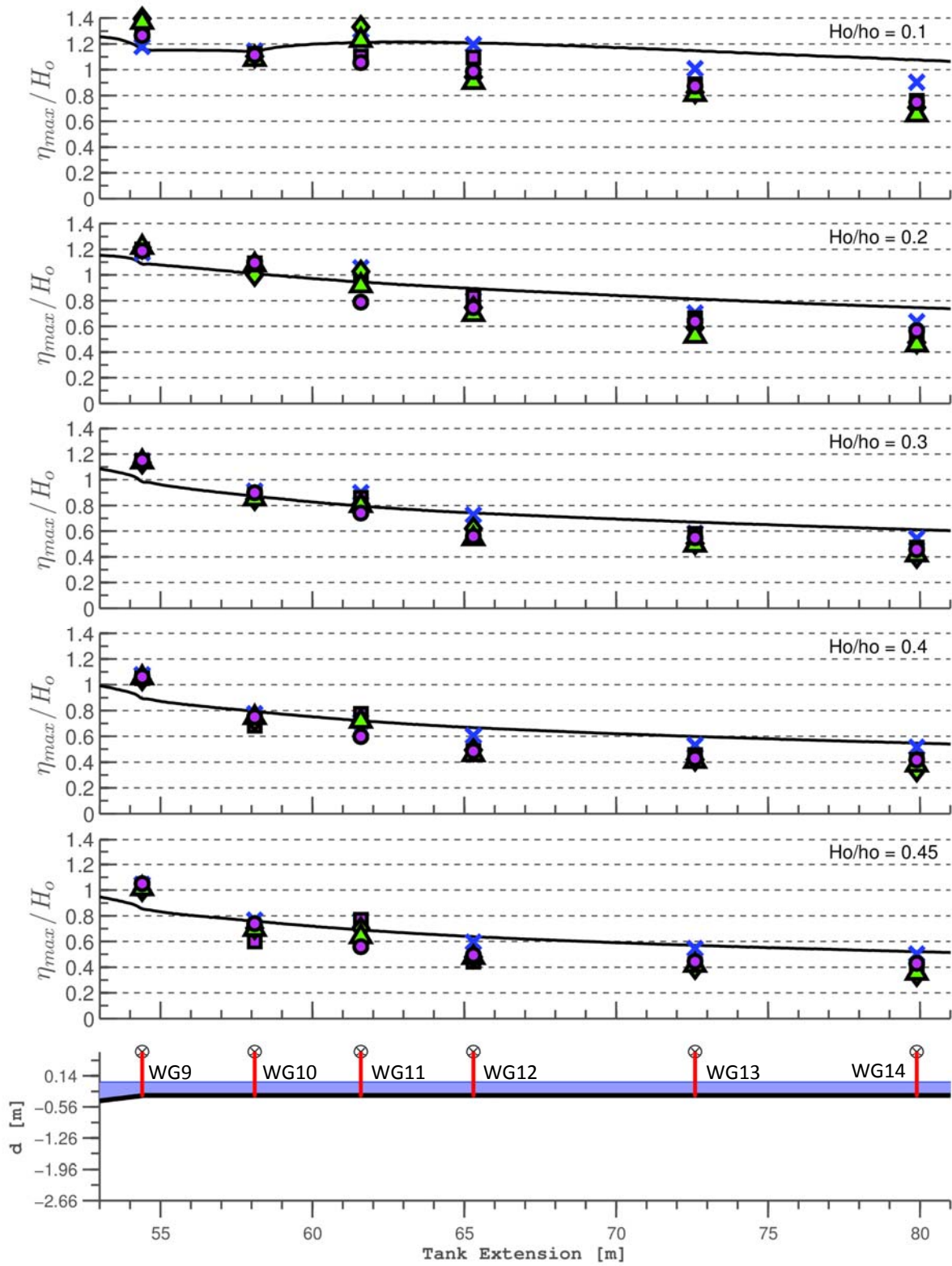


Figure 25. Normalized crest elevation along the flat reef with $h_f = 0.3$ m (-X- BF0, ■ BF1, ◆ BF2, ▲ BF3, ● BF4) and computed solution (- solid line) at 30 cm water level from the flat reef.

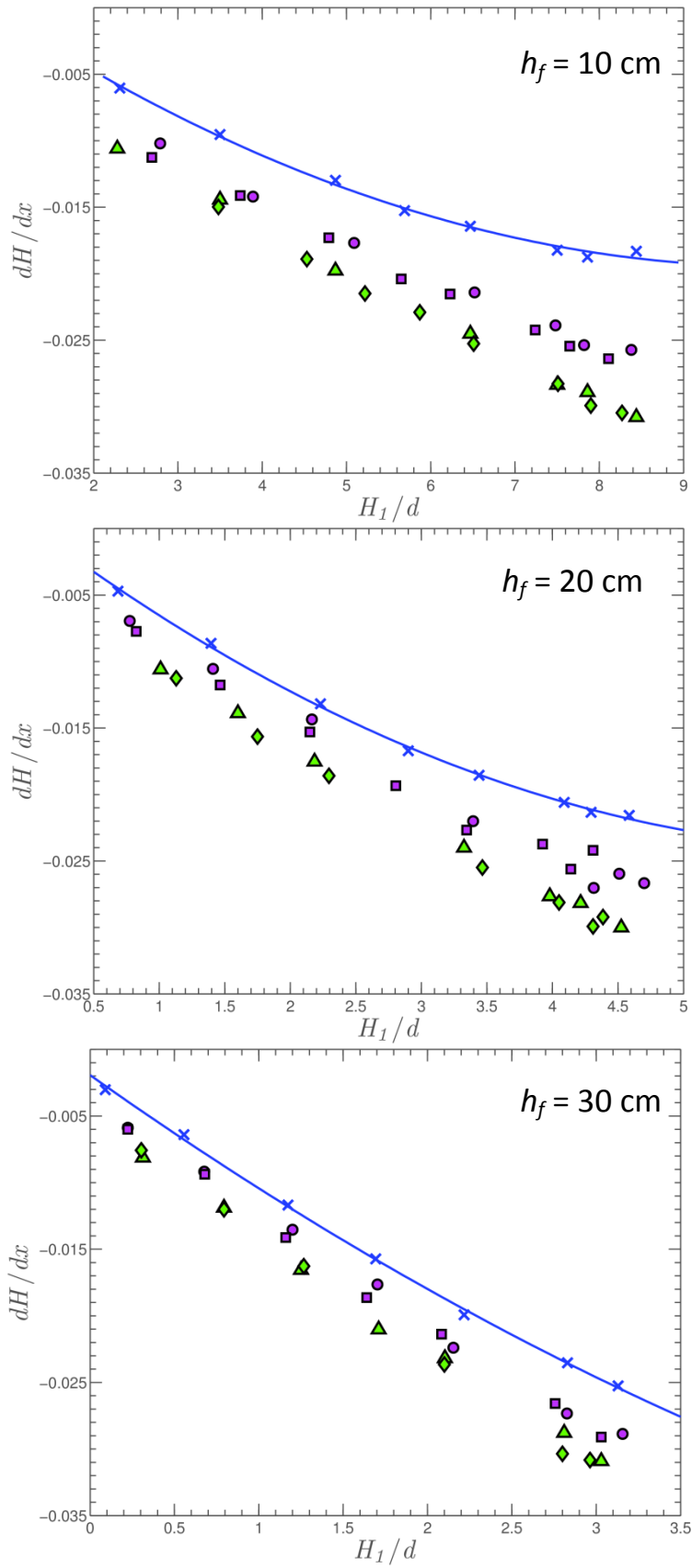


Figure 26. Wave height gradient between WG9 ($x = 54.4$ m) and wg14 ($x = 79.9$ m) on the flat reef (-X- BF0, ■ BF1, ◆ BF2, ▲ BF3, ● BF4).

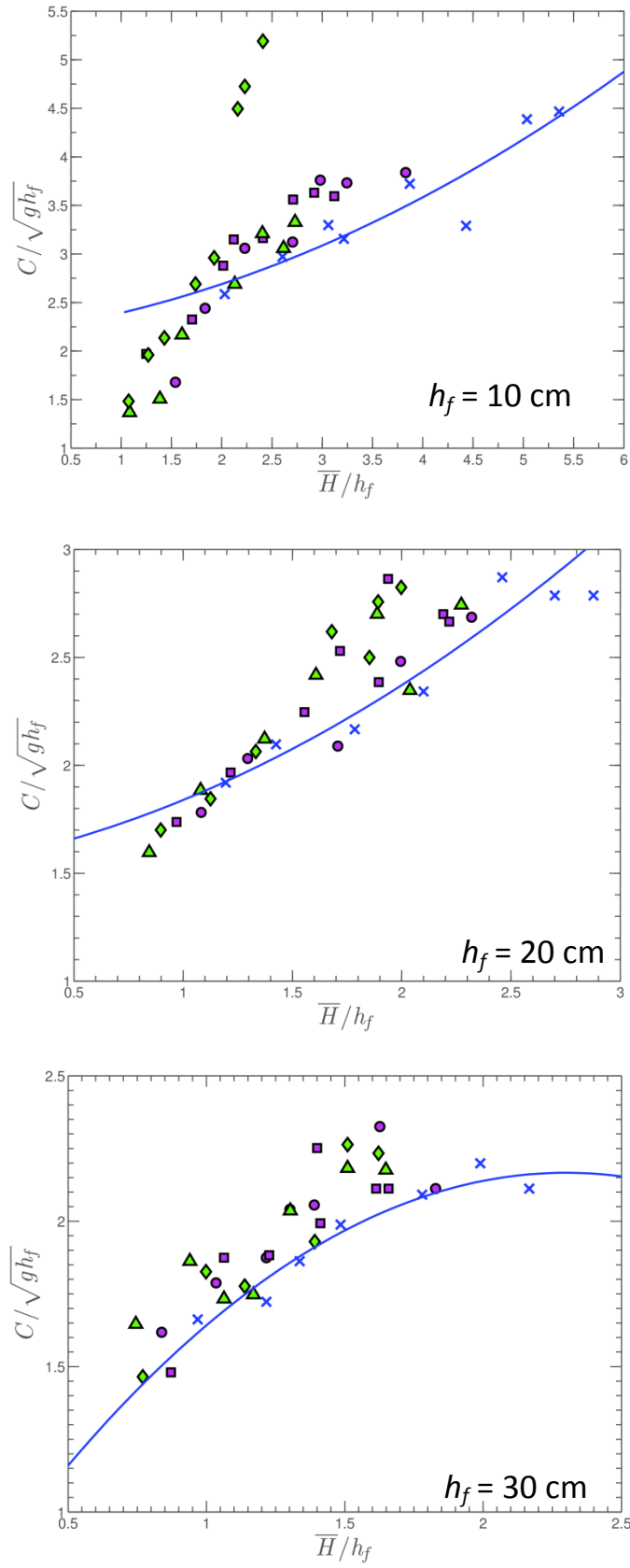


Figure 27. Average celerity between WG9 ($x = 54.4$ m) and WG14 ($x = 79.9$ m) on the flat reef (-X- BF0, \blacksquare BF1, \blacklozenge BF2, \blacktriangle BF3, \bullet BF4).